

# Einstein-Podolsky-Rosen Steering Using Single-Phonon Path Entanglement and Parity-Based Detection

Mathis Moes

ETH Zurich

September 8, 2022

## Abstract

Nonlocality in quantum mechanics can be categorized into three types: quantum entanglement, Einstein-Podolsky-Rosen steering, and Bell's nonlocality. Understanding these types of correlations is crucial for both fundamental research and future quantum technologies. In 1935, Erwin Schrödinger introduced the concept of steering in reply to the Einstein-Podolsky-Rosen (EPR) paradox. Surprisingly, it was only recently that EPR-steering was defined as a quantum information task for arbitrary bipartite states and measurements [1, 2]. In this project, we sought to investigate the demonstration of EPR steering between two mechanical resonators, for displacement-based and parity-based phonon number detection. First, we were able to observe how different variables such as the minimum required state purity  $\eta_*$  depend on the type of measurement, the number of measurement settings as well as on the measurement displacement amplitude  $r$ . We discovered that when considering parity-based measurements, a periodic pattern with respect to  $r$  occurred. This could be seen for the detection efficiency  $\eta_*$  as well as for the bound value  $S'_{max}$  of the corresponding steering inequality. In addition, we tested our numerical approach to detect steering on a simulated density matrix with realistic experimental parameters and imperfections. We were able to show for which  $r$  it turned out to be steerable respectively unsteerable considering parity and displacement-based measurements for a 2 level system.

## Contents

|          |   |           |
|----------|---|-----------|
| <b>1</b> | <b>Introduction</b>                             | <b>3</b>  |
| 1.1      | Overview . . . . .                              | 3         |
| 1.2      | Definition of quantum steering . . . . .        | 4         |
| 1.3      | Semidefinite program . . . . .                  | 7         |
| <b>2</b> | <b>Detection of quantum steering</b>            | <b>10</b> |
| 2.1      | Displacement-based measurements . . . . .       | 11        |
| 2.2      | Parity-based measurements . . . . .             | 12        |
| 2.3      | Testing simulated density matrix . . . . .      | 13        |
| 2.4      | Steering inequality . . . . .                   | 14        |
| <b>3</b> | <b>Results &amp; Discussion</b>                 | <b>15</b> |
| 3.1      | Displacement-based measurements . . . . .       | 15        |
| 3.2      | Parity-based measurements . . . . .             | 16        |
| 3.3      | Testing simulated density matrix . . . . .      | 24        |
| 3.4      | Steering inequality . . . . .                   | 27        |
| 3.4.1    | Dual SDP result . . . . .                       | 27        |
| 3.4.2    | Steering inequalities . . . . .                 | 28        |
| <b>4</b> | <b>Conclusion</b>                               | <b>29</b> |
| <b>A</b> | <b>Definitions and calculation steps</b>        | <b>34</b> |
| <b>B</b> | <b>SDP</b>                                      | <b>37</b> |
| <b>C</b> | <b>Dual SDP</b>                                 | <b>43</b> |
| C.1      | Duality theory . . . . .                        | 43        |
| C.2      | Derivation . . . . .                            | 43        |
| C.2.1    | Primal . . . . .                                | 43        |
| C.2.2    | Dual . . . . .                                  | 46        |
| C.3      | Calculation . . . . .                           | 48        |
| C.3.1    | Primal . . . . .                                | 48        |
| C.3.2    | Dual . . . . .                                  | 48        |
| C.3.3    | MATLAB code . . . . .                           | 54        |
| <b>D</b> | <b>Wigner function</b>                          | <b>58</b> |
| D.1      | Definition of Wigner function . . . . .         | 58        |
| D.2      | Analytical computation . . . . .                | 59        |
| D.3      | Bell's Inequality and Wigner Function . . . . . | 60        |

# 1 Introduction

## 1.1 Overview

In 1935, Albert **Einstein**, Boris **Podolsky** and Nathan **Rosen** (**EPR**) presented their argument that the description of the physical reality provided by quantum mechanics was incomplete and in conflict with the notion of locality and reality. Indeed, if local realism is valid, then quantum mechanics cannot be regarded as a complete theory to describe physical reality. Apart from its fundamental importance, this study had profound consequences: It was the first time that physicists recognized the unusual events associated with *entanglement*, which later on confirmed to be the one of the core concepts of current quantum information science. In their thought experiment they consider a pair of particles prepared in a so-called entangled state, and the local measurement of their position or momentum. The correlations in the state allow one then to predict the results of these measurements on the other party, under the condition that the same measurement is performed. They claimed that no action made on the first particle could have an immediate effect on the second, as that would require information to be transferred faster than light, which is prohibited by the theory of relativity. By introducing a principle known as the *EPR criterion of reality*, they deduced that the second particle must have a specific location respectively momentum value before either can be measured.

This stood in contrast to the views of Niels Bohr and Werner Heisenberg, who claimed that a quantum particle does not have a definite value for an attribute like momentum until it is measured. In order to interpret this "*spooky action at distance*", Erwin Schrödinger introduced the concept of quantum entanglement and quantum steering, referring to the idea that in a 2-particle scenario, one of the parties can alter the state of the other distant party by performing local measurements. Quantum entanglement, according to Schrödinger, is "*the characteristic trait of quantum mechanics*" that distinguishes quantum theory from classical theory. In 1964, John Stewart Bell suggested an inequality for *local hidden variable* (LHV) models. With the violation of the so-called Bell's inequality by quantum entangled states one could deduce the presence of Bell correlations, that are associated to the impossibility of describing nature with a local realistic theory.

Another breakthrough was the introduction of a new categorization of quantum nonlocality by Wiseman, Jones, and Doherty [3], which formalised the idea of steering proposed by Schrödinger in 1935. They stated that every demonstration of the EPR paradox<sup>1</sup>, as proposed

---

<sup>1</sup>The EPR paradox is a term used to describe the scenario presented by EPR. Nevertheless, the authors did not seek to bring out an actual paradox. Rather, they contended that quantum mechanics was an incomplete

by Reid [5], is likewise a demonstration of steering. While that statement was generally valid, their proof was however inadequate. Cavalcanti *et al.* [3] not only provided the needed proof, but they were also able to demonstrate the converse: Any demonstration of steering is also a demonstration of the EPR paradox. In other words, the EPR paradox and steering are nonlocality concepts that are interchangeable. Finally, Wiseman, Jones, and Doherty established in Ref.[3] that EPR-steering represents a new kind of nonlocality intermediate between entanglement and Bell-nonlocality. The difference between them could be explained with the matter of trust shared between the different parties. Apart from its theoretical significance, this categorization showed to be important in the following decades in the context of quantum communication and information [1, 4, 6, 7, 8, 9, 10, 11, 12, 13, 14, 15].

## 1.2 Definition of quantum steering

Quantum steering is a form of bipartite quantum correlation, intermediate to the concepts of entanglement and Bell non-locality. Indeed, quantum entanglement is a superset of steering, and Bell's nonlocality is a subset of steering. These notions are illustrated in Figure 1 and 2. Nonetheless, only steering, out of the three forms of quantum nonlocality, can show asymmetry in the correlations. In fact, in the case of entanglement and Bell nonlocality, Alice and Bob can be freely interchanged. However, this symmetric situation changes radically for the EPR steering scenario. For some asymmetric bipartite quantum states, Alice may be able to steer Bob, but Bob will never be able to steer Alice, or vice-versa. Some one-way quantum information tasks, such as quantum cryptography, might benefit from this very peculiar property [6].

In the following paragraph, we will explain how one party, let us say Alice, is able to remotely steer the state of another party's system by performing a local measurement on a shared quantum state. This effect enables the second party, which we will refer to as Bob from here on, to verify that the shared state is indeed entangled without having any knowledge about the measurements executed by Alice. It is often said that Alice represents an *untrusted party*, since Alice measures her system with an uncharacterized measurement, leaving Bob with an ensemble of unnormalized states, a so-called *assemblage*.

Let us now consider a bipartite situation in which Alice and Bob share an unknown quantum state  $\rho_{AB}$ . Alice can conduct  $n_A$  measurements on her subsystem, each having  $m_A$  possible

---

theory, in that it did not completely describe reality. Schrödinger appears to be the first to call the situation a *paradox*, because he could not accept that quantum mechanics was actually incomplete with EPR, but he could not identify a problem in their reasoning either. In retrospect, we now know that, while the argument is valid, one of the premises, in fact local causality, is wrong, which was proven by Bell [4].

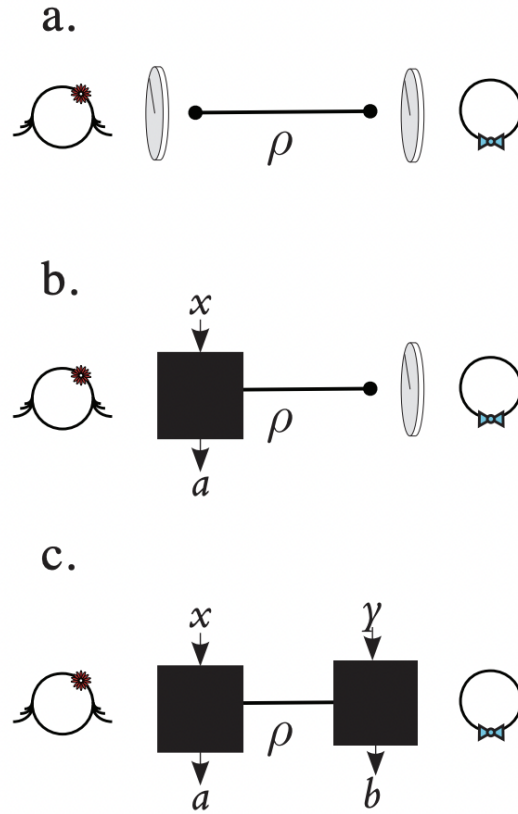


Figure 1: Schematic scenarios where entanglement can be verified. **a. Entanglement case:** Alice (left) and Bob (right) can apply a tomographically complete set of measurements in order to retrieve  $\rho_{AB}$ . **b. Quantum steering case:** Alice treats her measurements as a black box with inputs  $x$  and outputs  $a$ . Bob can then conduct tomography to reconstruct the set of states  $\sigma_{a|x}$  which are conditioned to Alice's measurements. **c. Quantum non-locality case:** Alice as well as Bob treat their measurements as black boxes [6].

outcomes  $a = 1, \dots, m_A$ . The state of Bob's system will then be changed into the conditional state  $\rho_{a|x}$  with probability  $p(a|x)$  after Alice having selected the measurement  $x$  and obtaining the outcome  $a$ . The steering scenario thus describes the situation in which Alice's measurements are not assumed to follow the rules of quantum mechanics, while Bob has complete trust over his quantum system, allowing him to access his conditional states by full tomography. In this case, the accessible information is a collection of post-measured states and their conditional probabilities, which are given by  $\{\rho_{a|x}, p(a|x)\}_{a,x}$ . This information can be summarized by a set of unnormalized quantum states, often referred to as an *assemblage*.

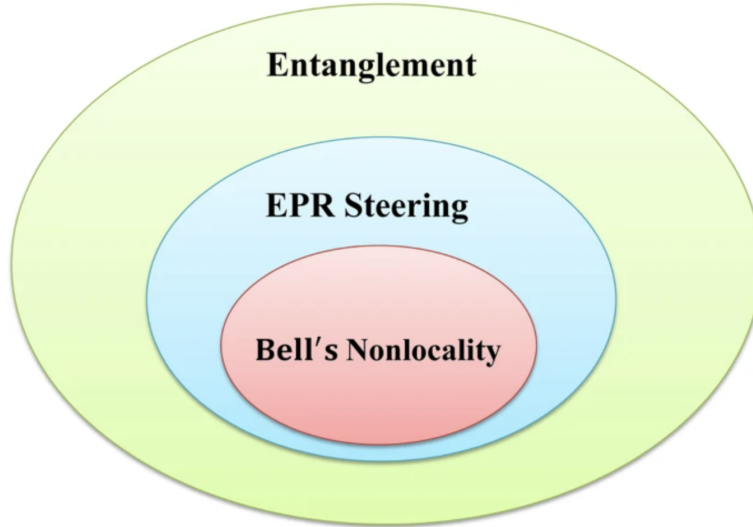


Figure 2: The strongest sort of quantum nonlocality is Bell's nonlocality. If a state has EPR steerability or Bell's nonlocality, it is certain to be entangled. EPR steering is a nonlocality that falls in between entanglement and Bell nonlocality [1].

Based on quantum theory, the terms of such an assemblage can then be acquired by

$$\sigma_{a|x} = \text{tr} [\rho_{AB}(M_{a|x} \otimes \mathbf{1})]. \quad (1)$$

$\sigma_{a|x}$  represents Bob's (unnormalized) state when Alice measures  $x$  and receives the outcome  $a$ , which can be expressed by the measurement operator  $M_{a|x}$ . In addition, we have the condition that  $\sum_a M_{a|x} = \mathbf{1}$  and that  $M_{a|x} \geq 0 \forall a, x$ . It is critical to emphasize that in the steering case, both the state  $\rho_{AB}$  and the measurement operators  $\{M_{a|x}\}_{a,x}$  are completely arbitrary.

In 2007, Wiseman, Jones and Doherty rigorously defined the concept of quantum steering as the possibility of generating remotely ensembles that could **not** be produced by a *local hidden state* (LHS) model. A LHS model describes a situation in which a source provides a classical message  $\lambda$  to one of the parties, Alice, and a quantum state  $\sigma_\lambda$  to the other party, Bob. The variable  $\lambda$  informs Alice's measuring device to output the result  $a$  with probability  $p(a|x, \lambda)$ , if she selects to consider the measurement  $x$ . Furthermore, it is assumed that the classical message  $\lambda$  can be chosen based on a distribution based on a density  $\pi(\lambda)$ . Since Bob does not have access to the classical variable  $\lambda$ , the final assemblage he sees is made up of the elements:

$$\sigma_{a|x} = \int d\lambda \pi(\lambda) p(a|x, \lambda) \sigma_\lambda \quad \forall a, x, \quad (2)$$

where  $\sigma_\lambda$  denotes the LHS, i.e. some quantum states, and  $p(a|x, \lambda)$  Alice's response function.

Thus, the dependence of Bob's state on Alice's measurement results **does not** indicate *spooky action at a distance*, if there exists a set of normalized states  $\sigma_\lambda$  with probability distribution  $\pi(\lambda)$  and  $p(a|x, \lambda)$  such that (2) holds. In that situation, we may be assured that Bob's system was always in a fixed state, and Alice's measurement result just provided us the classical information about  $\lambda$ . An assemblage that admits a decomposition of the form (2) can thus be reproduced by a LHS model, and is termed *unsteerable* as steering cannot be demonstrated. On the contrary, if Bob's observed assemblage **cannot** be brought in the form (2) for all  $a, x$ , then steering has been demonstrated, as no LHS model could reproduce the observed correlations. The assemblage is then said to be *steerable*.

To conclude, to verify steering, Bob must examine whether there exists a collection of quantum states  $\sigma_\lambda$ , a distribution  $\pi(\lambda)$  and  $p(a|x, \lambda)$  such that (2) holds. Analogous to Bell nonlocality and Bell inequalities, steering can be detected via violation of so-called *steering inequalities* [6, 11, 16, 17, 18, 19, 20, 21].

In essence, this is a complex challenge since the variable  $\lambda$  can take on an endless number of values. We will illustrate in the following subsection how this issue becomes significantly easier if the number of measurements and outputs is finite and how it then can be solved using semidefinite programming (SDP) [6].

### 1.3 Semidefinite program

In this subsection, we recap as outlined in Ref.[17] a numerical procedure to obtain the minimum purity required to observe steering with an entangled state. Assume that  $x = 1, \dots, n_A$  and  $a = 1, \dots, m_A$ , i.e. Alice performs  $n_A$  measurements with  $m_A$  possible outcomes each on the state

$$\rho_{AB}(\eta) = \eta |\Psi\rangle\langle\Psi| + (1 - \eta) |0, 0\rangle\langle 0, 0|, \quad (3)$$

where  $\eta$  parameterises the purity and

$$|\Psi\rangle = \frac{1}{\sqrt{2}} (|0, 1\rangle + |1, 0\rangle) \quad (4)$$

denotes a single-phonon entangled state. For given positive operator-valued measure (POVM) elements  $\Pi_{a|x}$ , Alice will steer Bob's state into the assemblage  $\{\sigma_{a|x}\}_{a,x}$  after completing measurement  $x$  on the state (3) and acquiring the outcome  $a$ . This assemblage can be computed in the following way according to [17]:

$$\sigma_{a|x}(\eta) = \text{Tr}_A(\rho_{AB}(\eta)\Pi_{a|x} \otimes \mathbb{1}) \quad (5)$$

$$= \eta\sigma_{a|x}^S + (1 - \eta)\sigma_{a|x}^{US}, \quad (6)$$

where we inserted (3) into (5) and the set of steerable respective unsteerable assemblages are given by the following expressions<sup>2</sup>:

$$\sigma_{a|x}^S = \text{Tr}_A(|\Psi\rangle\langle\Psi| \Pi_{a|x} \otimes \mathbb{1}), \quad (7)$$

$$\sigma_{a|x}^{US} = \text{Tr}_A(|0,0\rangle\langle 0,0| \Pi_{a|x} \otimes \mathbb{1}). \quad (8)$$

Now, one can notice that the  $p(a|x, \lambda)$  in (2) can be decomposed as a convex combination of a finite amount of deterministic probability distributions given a finite number of measurement choices and outcomes. Particularly, a deterministic probability distribution  $D_{\lambda'}(a|x)$  produces a fixed outcome  $a$  for each measurement  $x$ . This can be seen as  $D_{\lambda'}(a|x) = \delta_{a,\lambda'(x)}$ , such that  $a = \lambda'(x)$ . Here,  $\lambda'(\cdot)$  denotes a function from  $\{1, \dots, n_A\}$  to  $\{1, \dots, m_A\}$  and can be considered as a string of outcomes  $\lambda' = (a_{x=1}, \dots, a_{x=n_A})$ , such that  $\lambda'(x') = a_{x=x'}$ . Since there exist  $d = m_A^{n_A}$  such strings, i.e.  $d$  distinctive deterministic probability distributions, we can write:

$$p(a|x, \lambda) = \sum_{\lambda'=1}^d p(\lambda'|\lambda) D_{\lambda'}(a|x), \quad (9)$$

where  $p(\lambda'|\lambda)$  represents the weight of the deterministic distribution given by  $\lambda'$  in the case where the hidden variable is denoted by  $\lambda$  [6]. Recall that a LHS model describes the scenario in which a source sends a classical message  $\lambda$  to one of the parties, say Alice, and a corresponding quantum state  $\rho_\lambda$  to the other party, Bob.

Defining

$$\sigma_{\lambda'} := \int d\lambda \pi(\lambda) p(\lambda'|\lambda) \rho_\lambda, \quad (10)$$

---

<sup>2</sup>Note that (6), (7) and (8) only hold for this particular setup, which will enable us to acquire the minimum purity needed to observe steering with an entangled state. Later on in section 2.3, we will consider a more general case, where we cannot assume anymore that our density matrix can be decomposed into a set of steerable and unsteerable assemblages.



we can then write a LHS assemblage as

$$\sigma_{a|x} = \sum_{\lambda'=1}^d D_{\lambda'}(a|x)\sigma_{\lambda'}. \quad (11)$$

One might notice that (11) has a very similar form to (2). In the case of (11), we now have a finite sum instead of an integral and for each  $\lambda'$ , the deterministic probability distribution  $D_{\lambda'}(a|x)$  is fixed while for (2), the probabilities  $p(a|x, \lambda)$  were unknown. The case where we consider the number of measurements and outputs to be finite thus reduces the complexity of the construction of LHS assemblages.

In addition, one can note that

$$\text{Tr} \sum_{\lambda'} \sigma_{\lambda'} = \sum_{\lambda'} \int d\lambda \pi(\lambda) p(\lambda'|\lambda) = 1. \quad (12)$$

As a result, we can now formulate a *semidefinite programme* (SDP)[22] with the optimization variables  $\sigma_\lambda$  to determine if a given assembly  $\sigma_{a|x}$  with  $x = 1, \dots, n_A$  and  $a = 1, \dots, m_A$  is LHS. The SDP for this particular setup has the following form according to Ref.[17]:

$$\begin{aligned} \eta_* &\equiv \max \eta & 0 \leq \eta \leq 1 \\ \text{s.t.} & \sum_{\lambda} D_{\lambda}(a|x)\sigma_{\lambda} = \eta\sigma_{a|x}^S + (1-\eta)\sigma_{a|x}^{US} & \forall a, x \\ & \text{Tr} \sum_{\lambda} \sigma_{\lambda} = 1, \quad \sigma_{\lambda} \geq 0 & \forall \lambda. \end{aligned} \quad (13)$$

For a given set of POVM elements  $\Pi_{a|x}$ , which are needed to compute  $\sigma_{a|x}^S$  in (7) and  $\sigma_{a|x}^{US}$  in (8), we can then solve the above SDP numerically, which returns the critical value  $\eta_*$  above which the state  $\rho_{AB}(\eta)$  is steerable. In other words, (13) enables us to efficiently detect steering for the state (3) for all  $\eta$  down to the critical value

$$\eta \geq \eta_*. \quad (14)$$

We can now employ the duality theory to the previous problem (13) to obtain the dual problem. As shown in Appendix A in Ref.[6], by introducing dual Lagrangian variables, and moving to the Lagrangian, we acquire the following dual program:

$$\begin{aligned}
 S'_{max} &= \min \operatorname{Tr} \sum_{a,x} F_{a|x} \sigma'_{a|x} \\
 \text{s.t.} \quad &\sum_{a,x} F_{a|x} D_\lambda(a|x) \geq 0 \quad \forall \lambda \\
 \operatorname{Tr} \sum_{\lambda,a,x} &F_{a|x} D_\lambda(a|x) = 1.
 \end{aligned} \tag{15}$$

From the dual solution of the SDP, it is thus possible to extract the *steering functionals*  $F_{a|x}$  and the scalar  $S'_{max}$  [17]. These allows us to define the linear *steering inequality*, which is satisfied by all LHS assemblages<sup>3</sup>:

$$\operatorname{Tr} \sum_{a,x} F_{a|x} \sigma'_{a|x} \leq S'_{max}. \tag{16}$$

Any assemblage  $\{\sigma'_{a|x}\}_{a,x}$  providing a larger value than  $S'_{max}$  is steerable, and hence confirms that the shared state from which it was obtained is steerable [2, 6, 9, 17, 23, 24].

In Figure 3, we illustrate geometrically how the SDP and the steering inequality approach to detect steering. Let us consider two different sets, designated by US (the set of unsteerable assemblages) and S (the set of the steerable assemblages). For given POVM elements we have the two assemblages  $\{\sigma_{a|x}^{US}\}$  and  $\{\sigma_{a|x}^S\}$  in the corresponding sets. With (13), the obtained value  $\eta_*$  informs us about the "position of the boundary assemblage" separating the sets US and S. This is illustrated by  $\{\sigma_{a|x}(\eta_*)\}$  in Figure 3. The steering inequality (16), which is characterized by an assemblage  $\{\sigma'_{a|x}\}_{a,x}$ , represents a hyperplane and thus allows us to separate the set US from S. This is illustrated by the red line in 3. Thus, with this procedure, we can deduce that any assemblage  $\{\sigma'_{a|x}\}_{a,x}$  violating the steering inequality, i.e. being on the right side of the red line in Figure 3, is steerable, certifying that the shared state from which it was acquired was indeed entangled [17].

## 2 Detection of quantum steering

The first task of this project is to investigate the behaviour of the variable  $\eta_*$  for displacement-based as well as for parity-based measurements by means of the SDP (13) for different values

---

<sup>3</sup>For more details, we will refer to the papers [6] and [17].

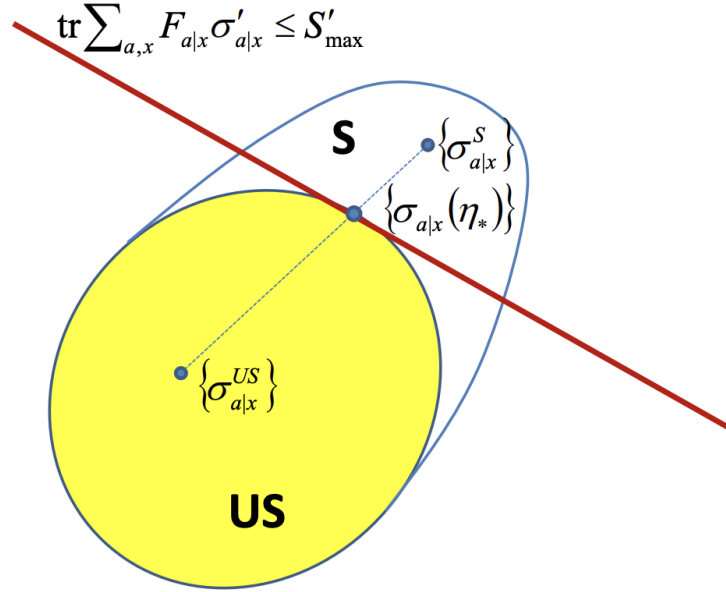


Figure 3: Geometric representation the unsteerable and steerable set of assemblages, designated by US and S respectively. The red line represents the hyperplane that corresponds to a steering inequality which is characterized by an assemblage  $\{\sigma'_{a|x}\}_{a,x}$ . Any such assemblage  $\{\sigma'_{a|x}\}_{a,x}$  identified on the right side of the red line comes out to be steerable [17].

of the measurement displacement amplitude  $r$ . We will consider a two-output ( $a = \pm 1$ ) steering scenario with both 2, 3 and 4 measurement settings  $x$  and multiple level systems.

## 2.1 Displacement-based measurements

We will first consider displacement-based measurements, which involve a displacement followed by single-phonon detection. Here, we will neglect phonon-number resolution.

Let us consider the projector

$$\Pi(\alpha) = |\alpha\rangle\langle\alpha|, \quad (17)$$

where  $|\alpha\rangle$  denotes the coherent state corresponding to the displacement  $\alpha = re^{i\theta}$  with  $r \geq 0$  being the measurement displacement amplitude and  $\theta \in [0, 2\pi]$  the phase. We suppose that a no-click outcome corresponds to this projector. A general expression for (17), restricting the Hilbert space to two levels, is given by (60) in Appendix A. By assigning the outcomes +1 (to the click event) and -1 (to the no-click event), a displacement measurement then corresponds

to the observable

$$M(\alpha) = 2|\alpha\rangle\langle\alpha| - \mathbf{1}. \quad (18)$$

The according POVM elements in the case where Alice performs the measurement setting  $x$  on the state (3) and obtains the result  $a \in \{-1, 1\}$  can then be described by the following expression:

$$\Pi_{a|x} = \frac{\mathbf{1} + aM(r, \theta_x)}{2}, \quad (19)$$

where  $\theta_x$  represents the phase belonging to the measurement  $x$  [17]. For a two level system, the general expression for (19) is given by:

$$\Pi_{a|x} = \frac{1}{2} \begin{pmatrix} 1 + a(2e^{-r^2} - 1) & 2are^{-r^2 - i\theta_x} \\ 2are^{-r^2 + i\theta_x} & 1 + a(2r^2e^{-r^2} - 1) \end{pmatrix}. \quad (20)$$

Table 1 displays the individual phases we will consider for the different measurement settings.

| Measurement settings $x$ | $\theta_x$ [rad.] |
|--------------------------|-------------------|
| 2                        | $\theta_1=0$      |
|                          | $\theta_2=\pi$    |
| 3                        | $\theta_1=0$      |
|                          | $\theta_2=2\pi/3$ |
|                          | $\theta_3=4\pi/3$ |
| 4                        | $\theta_1=0$      |
|                          | $\theta_2=\pi/2$  |
|                          | $\theta_3=\pi$    |
|                          | $\theta_4=3\pi/2$ |

Table 1: Phases  $\theta_x$  for the different measurement settings.

## 2.2 Parity-based measurements

We will now consider the scenario where the detectors are able to resolve the number of phonons. We assign +1 to the event where an even number of phonons have been counted and -1 to the opposite event, where an odd number has been registered. This measurement is described similar to the subsection above by a pair of projection operators given by the

following expressions:

$$\Pi^{(+)}(\alpha) = D(\alpha) \sum_{k=0}^{\infty} |2k\rangle\langle 2k| D^\dagger(\alpha), \quad (21)$$

$$\Pi^{(-)}(\alpha) = D(\alpha) \sum_{k=0}^{\infty} |2k+1\rangle\langle 2k+1| D^\dagger(\alpha). \quad (22)$$

In (21) and (22),  $D(\alpha)$  describes the displacement operator

$$D(\alpha) = \exp(\alpha \hat{a}^\dagger - \alpha^* \hat{a}), \quad (23)$$

with  $\hat{a}^\dagger$  and  $\hat{a}$  denoting the creation respectively annihilation operator, which can be represented by the matrices (63) and (64). Again, the phases in Table 1 for the different measurement settings  $x$  are considered.

The corresponding measurement can then be written as

$$M'(\alpha) = \Pi^{(+)} - \Pi^{(-)}, \quad (24)$$

which then allows us to acquire the expression of the appropriate POVM elements using (19):

$$\Pi'_{a|x} = \frac{\mathbb{1} + aM'(r, \theta_x)}{2}. \quad (25)$$

### 2.3 Testing simulated density matrix

Next, we analyse a simulated density matrix for two entangled mechanical resonators from *Michael Eichenberger*, which takes realistic experimental parameters and imperfections. With a modification of the SDP from (13), we can check whether it can be described by a LHS model or not, thus being unsteerable or not. Only displacement-based and parity-based measurements for a two-level system will be considered here. In order to compute this, we need to adapt some steps, which will be explained in the following lines.

First, we cannot assume that our density matrix can be splitted into a set of steerable and unsteerable assemblages anymore, as contrary to the analytical state considered before we do not have any a priori knowledge for the simulated state. Thus, we will operate with (5), where  $\rho_{AB}$  will represent our simulated density matrix. Next, since we are now interested whether the conditional state can be described by a LHS model, the SDP (13) will change

to:

$$\begin{aligned} \sum_{\lambda} D_{\lambda}(a|x)\sigma_{\lambda} &= \sigma_{a|x} = \text{Tr}_A(\rho_{AB}\Pi_{a|x} \otimes \mathbf{1}) \quad \forall a, x \\ \text{Tr} \sum_{\lambda} \sigma_{\lambda} &= 1, \quad \sigma_{\lambda} \geq 0 \quad \forall \lambda, \end{aligned} \quad (26)$$

where one notes that the maximization/minimization statement becomes unnecessary<sup>4</sup>. This SDP will then output whether for the specific density condition, a LHS model can be found or not, according to the possible statuses (feasible/unfeasible) given by CVX [25].

## 2.4 Steering inequality

Finally, we seek to investigate the behaviour of the steering inequalities with (16) for different cases. According to Ref.[17], the steering functionals  $F_{a|x}$  should be positive semidefinite and match the following *steering matrices*:

$$G'_R = \begin{pmatrix} s & 0 \\ 0 & 0 \end{pmatrix} \quad s > 0, \quad (27)$$

$$G'_x = \begin{pmatrix} 0 & te^{\frac{i(x-1)\pi}{4}} \\ te^{-\frac{i(x-1)\pi}{4}} & \frac{1}{4} \end{pmatrix} \quad \text{for } x = 1, 2, 3, 4 \quad t > 0, \quad (28)$$

where  $G'_R = \sum_{x=1}^4 F_{-|x}$  and  $G'_x = F_{+|x} - F_{-|x}$ .

---

<sup>4</sup>However, since CVX, a MATLAB-based modeling system for convex optimization [25], requires a maximization/minimization condition, we will simply employ a "trivial" statement in the code, i.e. `maximise(0)`.

### 3 Results & Discussion

In this section we report and discuss the results of our investigations of steering detection using different measurement types and system dimensions.

#### 3.1 Displacement-based measurements

For the displacement-based measurements, we will only consider a two-level system. Regarding the POVM elements (19), we can obtain the value  $\eta_*$  using the SDP from (13). Computing this SDP for different  $r$  yields the following Figure 4.

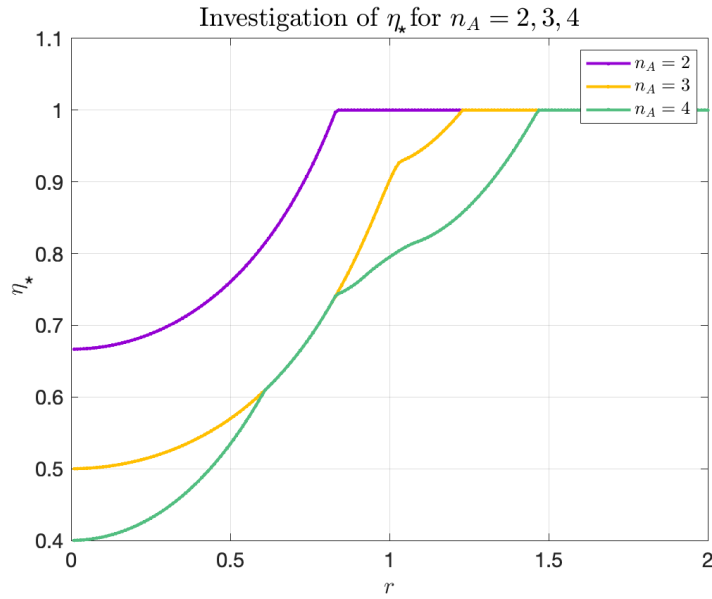


Figure 4: Plot of  $\eta_*$  against  $r$  for the two-level system for 2, 3 and 4 displacement-based measurement settings. The measurement setting phases are given in Table 1.

Looking at Figure 4, one can see that the value of  $\eta_*$  increases differently for the individual number of measurement settings and starts at different values for  $r = 0$ . In fact, one notices that for a higher number of measurement settings,  $\eta_*$  reaches value 1 for larger  $r$ , which can be interpreted in a way that now  $\sigma_{a|x}$  only consists of a set of steerable assemblages. Furthermore, one observes that at a certain value of  $r$ ,  $\eta_*$  will not noticeably change anymore. This makes sense since the POVM elements (19) are of the form:

$$\Pi_{a|x} = \frac{1}{2} \begin{pmatrix} 1 + 2ae^{-r^2} - a & 2are^{-r^2-i\theta} \\ 2are^{-r^2+i\theta} & 1 + 2ar^2e^{-r^2} - a \end{pmatrix}, \quad (29)$$

where we used the interim result (60). Thus, for  $r \rightarrow \infty$ , (29) will converge to

$$\Pi_{a|x} = \frac{1}{2} \begin{pmatrix} 1-a & 0 \\ 0 & 1-a \end{pmatrix}, \quad (30)$$

being independent of  $r$ . This therefore depicts why for large  $r$ ,  $\eta_*$  converges to a constant, in this case to the value 1. Finally, the curve for 3 measurements matches the one for 4 measurements in the approximate range from 0.6 to 0.8. However, I could not find a mathematical or physical explanation for this behaviour.

### 3.2 Parity-based measurements

In this subsection, we consider the parity-based measurements for 2, 3 and 4 level systems. Therefore, we proceed similarly as for the displacement-based measurements, but now we employ the parity-based POVM elements (25), yielding Figures 5, 6 and 7.

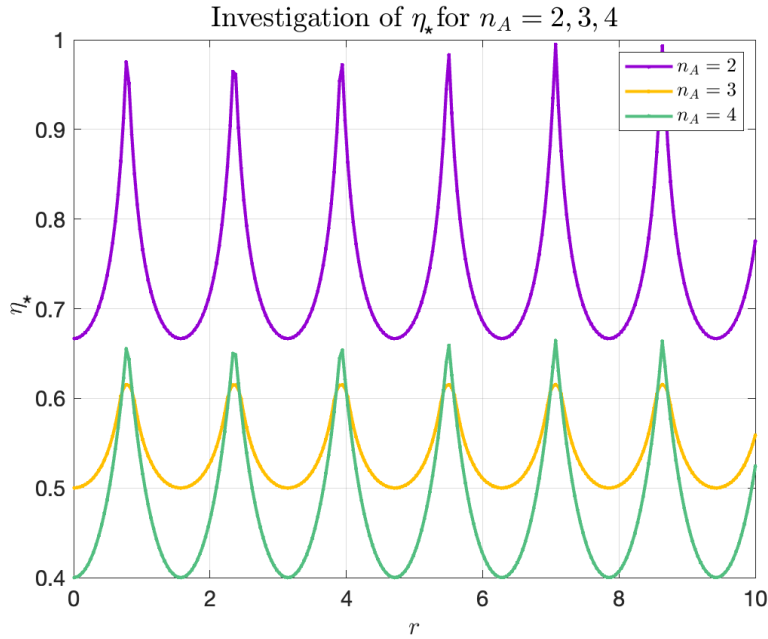


Figure 5: Plotting  $\eta_*$  against  $r$  for the 2 level system for 2, 3 and 4 parity-based measurement settings. The measurement setting phases are given in Table 1.

▷ First, we will discuss the 2 level system case. Regarding Figure 5, one notices an oscillating behaviour with respect to  $r$ . In the following, we seek to understand the origin of this periodic pattern.



The displacement operator for the 2 level system is specified by (23):

$$D(\alpha) = \exp \begin{pmatrix} 0 & -\alpha^* \\ \alpha & 0 \end{pmatrix}. \quad (31)$$

Defining  $X := \begin{pmatrix} 0 & -\alpha^* \\ \alpha & 0 \end{pmatrix}$ , we observe that:

$$X^2 = \begin{pmatrix} -\alpha^* \alpha & 0 \\ 0 & -\alpha^* \alpha \end{pmatrix},$$

$$X^3 = \begin{pmatrix} 0 & (\alpha^*)^2 \alpha \\ -\alpha^* \alpha^2 & 0 \end{pmatrix},$$

$$X^4 = \begin{pmatrix} (\alpha^*)^2 \alpha^2 & 0 \\ 0 & (\alpha^*)^2 \alpha^2 \end{pmatrix}.$$

Thus, one can write

$$X^{2k} = (-1)^k (\sqrt{\alpha^* \alpha})^{2k} \mathbf{1}, \quad (32)$$

$$X^{2k+1} = (-1)^{k+1} (\sqrt{\alpha^* \alpha})^{2k} X, \quad (33)$$

yielding<sup>5</sup>:

$$D(\alpha) = \exp(X) = \begin{pmatrix} \cos(r) & \sin(r)e^{i\theta} \\ -\sin(r)e^{-i\theta} & \cos(r) \end{pmatrix}. \quad (34)$$

---

<sup>5</sup>The detailed derivation for this can be found in Appendix A.

Now, this enables us to compute the projection operators (21) and (22):

$$\begin{aligned}\Pi^{(+)} &= D(\alpha) |0\rangle\langle 0| D(\alpha)^\dagger \\ &= \begin{pmatrix} \cos^2(r) & -\cos(r)\sin(r)e^{i\theta} \\ -\cos(r)\sin(r)e^{-i\theta} & \sin^2(r) \end{pmatrix},\end{aligned}\quad (35)$$

$$\begin{aligned}\Pi^{(-)} &= D(\alpha) |1\rangle\langle 1| D(\alpha)^\dagger \\ &= \begin{pmatrix} \sin^2(r) & \cos(r)\sin(r)e^{i\theta} \\ \cos(r)\sin(r)e^{-i\theta} & \cos^2(r) \end{pmatrix}.\end{aligned}\quad (36)$$

Remembering the trigonometric identities

$$2\sin^2(r) = 1 - \cos(2r),\quad (37)$$

$$2\sin(r)\cos(r) = \sin(2r),\quad (38)$$

$$\cos^2(r) + \sin^2(r) = 1,\quad (39)$$

and that  $\cos(2r)$  respectively  $\sin(2r)$  have a periodicity of  $\pi$ , we can conclude that both projection operators  $\Pi^{(+)}$  and  $\Pi^{(-)}$  are  $\pi$ -periodic, i.e. share the same periodicity. The POVM elements (25) are given by:

$$\Pi'_{a|x} = \frac{1}{2} \begin{pmatrix} 1 + a(\cos^2(r) - \sin^2(r)) & -2a\cos(r)\sin(r)e^{i\theta} \\ -2a\cos(r)\sin(r)e^{-i\theta} & 1 + a(\sin^2(r) - \cos^2(r)) \end{pmatrix}.\quad (40)$$

Accordingly, this explains why Figure 5 depicts a periodic behaviour. The periodicity in  $r$  can be interpreted in a way that the "steerability" of the considered state oscillates with respect to  $r$ .

▷ Next, we consider the 3 level system. Similar to the former case, Figure 6 displays a periodic pattern.

In this case, the displacement operator is given by:

$$D(\alpha) = \exp \underbrace{\begin{pmatrix} 0 & -\alpha^* & 0 \\ \alpha & 0 & -\sqrt{2}\alpha^* \\ 0 & \sqrt{2}\alpha & 0 \end{pmatrix}}_{:=X}.\quad (41)$$

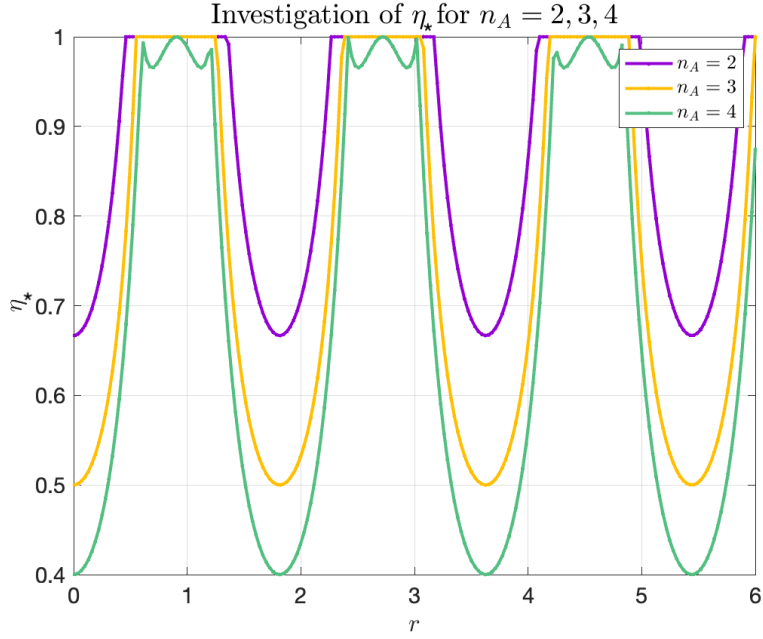


Figure 6: Plotting  $\eta_*$  against  $r$  for the 3 level system for 2, 3 and 4 parity-based measurement settings. The measurement setting phases are given in Table 1.

Now, we seek to diagonalize the matrix  $X = PJP^{-1}$ , where  $P$  is a matrix composed of the eigenvectors of  $X$ ,  $J$  is the diagonal matrix constructed from the corresponding eigenvalues, and  $P^{-1}$  is the matrix inverse of  $P$ .

We find:

$$P = \begin{pmatrix} \frac{\sqrt{2}\alpha^*}{\alpha} & \frac{-\alpha^*}{\sqrt{2}\alpha} & \frac{-\alpha^*}{\sqrt{2}\alpha} \\ 0 & -\frac{i\sqrt{\frac{3}{2}}\sqrt{\alpha^*}}{\sqrt{\alpha}} & \frac{i\sqrt{\frac{3}{2}}\sqrt{\alpha^*}}{\sqrt{\alpha}} \\ 1 & 1 & 1 \end{pmatrix}, \quad (42)$$

$$J = \begin{pmatrix} 1 & 0 & 0 \\ 0 & e^{-i\sqrt{3}\alpha\alpha^*} & 0 \\ 0 & 0 & e^{i\sqrt{3}\alpha\alpha^*} \end{pmatrix}, \quad (43)$$

$$P^{-1} = \begin{pmatrix} \frac{\sqrt{2}\alpha}{3\alpha^*} & 0 & \frac{1}{3} \\ -\frac{\alpha}{3\sqrt{2}\alpha^*} & \frac{i\sqrt{\alpha}}{\sqrt{6}\sqrt{\alpha^*}} & \frac{1}{3} \\ -\frac{\alpha}{3\sqrt{2}\alpha^*} & -\frac{i\sqrt{\alpha}}{\sqrt{6}\sqrt{\alpha^*}} & \frac{1}{3} \end{pmatrix}. \quad (44)$$

With those, we can then compute  $D(\alpha)$ , yielding:

$$D(\alpha) = \begin{pmatrix} \frac{1}{3} \cos(\sqrt{3}r) + \frac{2}{3} & -\frac{1}{\sqrt{3}} e^{-i\theta} \sin(\sqrt{3}r) & -\frac{2}{3\sqrt{2}} e^{-2i\theta} \cos(\sqrt{3}r) + \frac{\sqrt{2}}{3} e^{-2i\theta} \\ \frac{1}{\sqrt{3}} e^{i\theta} \sin(\sqrt{3}r) & \cos(\sqrt{3}r) & -\frac{2}{\sqrt{6}} e^{-i\theta} \sin(\sqrt{3}r) \\ -\frac{2}{3\sqrt{2}} e^{2i\theta} \cos(\sqrt{3}r) + \frac{\sqrt{2}}{3} e^{2i\theta} & \frac{2}{\sqrt{6}} e^{i\theta} \sin(\sqrt{3}r) & \frac{2}{3} \cos(\sqrt{3}r) + \frac{1}{3} \end{pmatrix}.$$

This enables us now to calculate the parity projection operators (21) and (22) accordingly:

$$\Pi^{(+)} = D(\alpha) [ |0\rangle\langle 0| D(\alpha)^\dagger + |2\rangle\langle 2| D(\alpha)^\dagger ], \quad (45)$$

$$\Pi^{(-)} = D(\alpha) [ |1\rangle\langle 1| D(\alpha)^\dagger ]. \quad (46)$$

Those yield the following matrices:

$$\Pi^{(+)} = \begin{pmatrix} \frac{\cos(2\sqrt{3}r)}{6} + \frac{5}{6} & \frac{\sqrt{3} \sin(2\sqrt{3}r) (\cos(\theta) - \sin(\theta)i)}{6} & -\frac{\sqrt{2} e^{-2i\theta} (\cos(2\sqrt{3}r) - 1)}{6} \\ \frac{\sqrt{3} \sin(2\sqrt{3}r) (\cos(\theta) + \sin(\theta)i)}{6} & \sin^2(\sqrt{3}r) & -\frac{\sqrt{6} \sin(2\sqrt{3}r) (\cos(\theta) - \sin(\theta)i)}{6} \\ -\frac{\sqrt{2} e^{2i\theta} (\cos(2\sqrt{3}r) - 1)}{6} & -\frac{\sqrt{6} \sin(2\sqrt{3}r) (\cos(\theta) + \sin(\theta)i)}{6} & \frac{\cos(2\sqrt{3}r)}{3} + \frac{2}{3} \end{pmatrix}, \quad (47)$$

$$\Pi^{(-)} = \begin{pmatrix} \frac{\sin(\sqrt{3}r)^2}{3} & -\frac{\sqrt{3} \sin(2\sqrt{3}r) (\cos(\theta) - \sin(\theta)i)}{6} & -\frac{\sqrt{2} e^{-\theta 2i} \sin(\sqrt{3}r)^2}{3} \\ -\frac{\sqrt{3} \sin(2\sqrt{3}r) (\cos(\theta) + \sin(\theta)i)}{6} & \cos^2(\sqrt{3}r) & \frac{\sqrt{6} \sin(2\sqrt{3}r) (\cos(\theta) - \sin(\theta)i)}{6} \\ -\frac{\sqrt{2} e^{\theta 2i} \sin(\sqrt{3}r)^2}{3} & \frac{\sqrt{6} \sin(2\sqrt{3}r) (\cos(\theta) + \sin(\theta)i)}{6} & \frac{2 \sin(\sqrt{3}r)^2}{3} \end{pmatrix}. \quad (48)$$

Here, one realizes that the two operators again share the same periodicity, which is given by  $\frac{\pi}{\sqrt{3}}$ . Thus we acquire periodic POVM elements using (25). This explains therefore the origin of the periodic pattern in Figure 6.

▷ We will not consider the last case for 4 levels as in detail, since the calculations become too complicated.

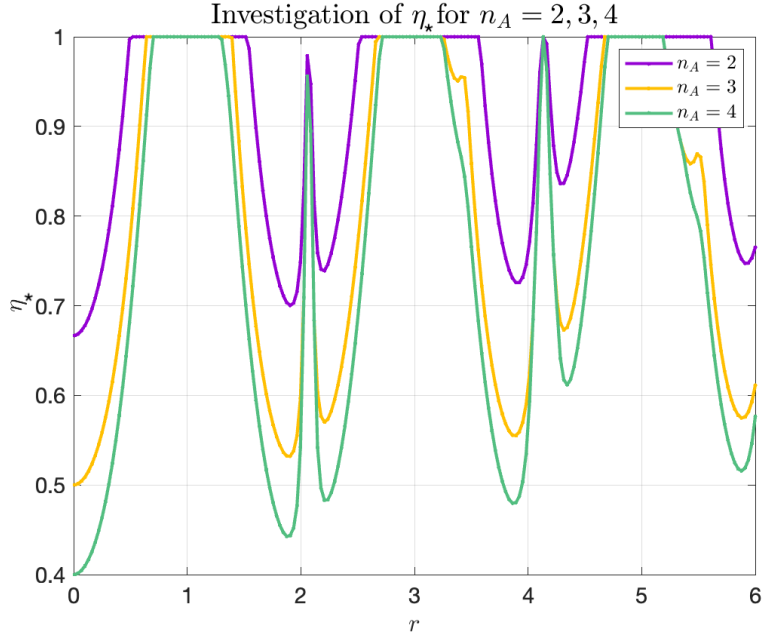


Figure 7: Plotting  $\eta_*$  against  $r$  for the 4 level system for 2, 3 and 4 parity-based measurement settings. The measurement setting phases are given in Table 1. The same plot with a larger range is depicted in 8 in order to see the periodicity of  $\eta_*$  with respect to  $r$  more clearly.

At first, one is not able to observe a periodic behaviour as can be seen in Figure 7. However, when considering a larger range, we obtain Figure 8, enabling us to notice a periodic pattern in  $r$ .

The displacement operator in this case is given by:

$$D(\alpha) = \exp \begin{pmatrix} 0 & -\sqrt{1}\alpha^* & 0 & 0 \\ \sqrt{1}\alpha & 0 & -\sqrt{2}\alpha^* & 0 \\ 0 & \sqrt{2}\alpha & 0 & -\sqrt{3}\alpha^* \\ 0 & 0 & \sqrt{3}\alpha & 0 \end{pmatrix}. \quad (49)$$

The corresponding projection operators (21) and (22) are then specified by:

$$\Pi^{(+)} = D(\alpha) [ |0\rangle\langle 0| D(\alpha)^\dagger + |2\rangle\langle 2| D(\alpha)^\dagger ], \quad (50)$$

$$\Pi^{(-)} = D(\alpha) [ |1\rangle\langle 1| D(\alpha)^\dagger + |3\rangle\langle 3| D(\alpha)^\dagger ], \quad (51)$$

which we will not compute explicitly. We can however assume that the two projection oper-

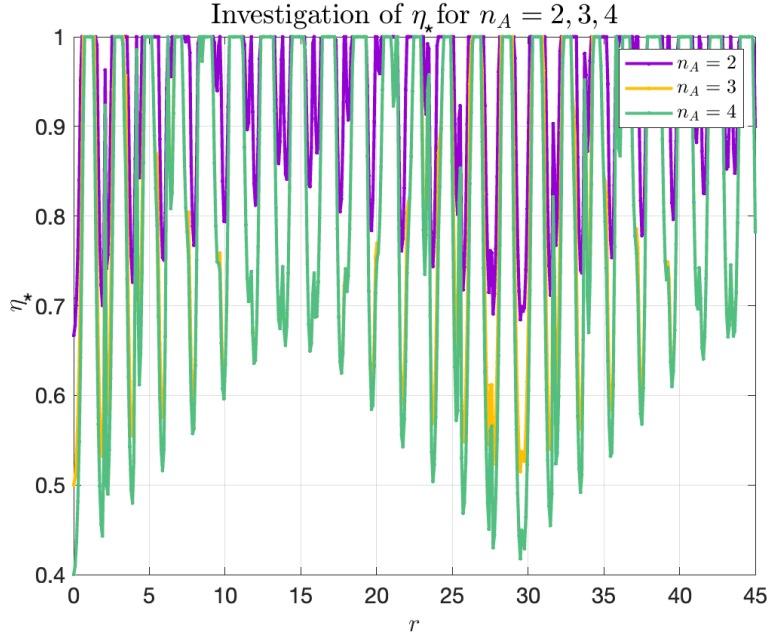


Figure 8: Figure 7 for a larger range. Here, one can see the periodic behaviour more clearly.

ators (21) and (22) also share the same periodicity as was shown for the 2 and 3 level system cases, demonstrating and manifesting the periodic pattern as depicted in Figure 8.

To summarize, the 2, 3 and 4 level systems for parity-based measurements display a periodic behaviour of  $\eta_*$ , which can be interpreted as an oscillation of the steerability of the considered state. These oscillations, however, can be seen as originating from the truncation of the Hilbert space, and are not expected to occur in a continuous-variable system.

Finally, Figure 9 allows us to see the different data in the same graph and thus to compare the different curves.

One notices that the different curves for the corresponding number of measurement settings  $x$  converge to the same value of  $\eta_*$  for  $r = 0$ . We will investigate this in further detail.

From (29) and (40), we obtain the following POVM elements for 2 levels and displacement and parity-based measurements:

$$\Pi_{a|x} = \frac{1}{2} \begin{pmatrix} 1 + 2ae^{-r^2} - a & 2are^{-r^2-i\theta} \\ 2are^{-r^2+i\theta} & 1 + 2ar^2e^{-r^2} - a \end{pmatrix} \xrightarrow{r=0} \frac{1}{2} \begin{pmatrix} 1 + a & 0 \\ 0 & 1 - a \end{pmatrix}, \quad (52)$$

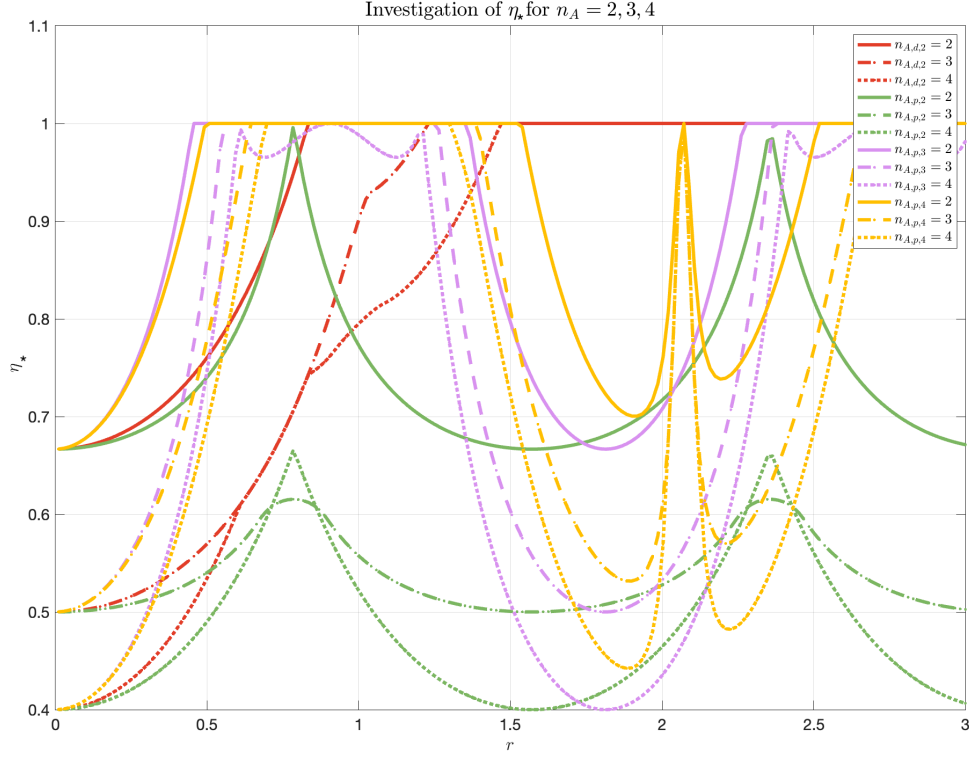


Figure 9: Combined curves from Figures 4, 5, 6, 7 in the range  $r \in [0, 3]$ . Here,  $n_{A,d,i}$  describes the number of measurement settings for the displacement-based measurement and the  $i$  level system, while  $n_{A,p,i}$  represents the number of measurement settings for the parity-based measurement and the  $i$  level system.

$$\Pi'_{a|x} = \frac{1}{2} \begin{pmatrix} 1 + a(\cos^2(r) - \sin^2(r)) & -2a \cos(r) \sin(r) e^{i\theta} \\ -2a \cos(r) \sin(r) e^{-i\theta} & 1 + a(\sin^2(r) - \cos^2(r)) \end{pmatrix} \xrightarrow{r=0} \frac{1}{2} \begin{pmatrix} 1 + a & 0 \\ 0 & 1 - a \end{pmatrix}. \quad (53)$$

Next, we can compute the POVM elements for  $r=0$  for the 3 level system and parity-based measurements with (47) and (48), yielding:

$$\Pi^{(+)} = \begin{pmatrix} 1 & 0 & 0 \\ 0 & 1 & 0 \\ 0 & 0 & 1 \end{pmatrix}, \quad \Pi^{(-)} = \begin{pmatrix} 0 & 0 & 0 \\ 0 & 1 & 0 \\ 0 & 0 & 0 \end{pmatrix} \quad (54)$$

Then, using (24) and (25), we get:

$$\Pi'_{a|x} = \frac{1}{2} \begin{pmatrix} 1+a & 0 & 0 \\ 0 & 0 & 0 \\ 0 & 0 & 1-a \end{pmatrix}. \quad (55)$$

We can further assume that we obtain a similar matrix for the 4 level case, which we will however not calculate here.

From the similar matrix entries, one could deduce the corresponding convergence for the different curves at  $r = 0$ .

### 3.3 Testing simulated density matrix

In parallel with this project, another master student simulated the preparation of multipartite entangled states in the high-overtone bulk acoustic wave resonators investigated by the group of Prof. Y. Chu. In particular, he simulated the preparation of  $|01\rangle + |10\rangle$  entangled states, which resulted in the density matrix:

$$\rho_{AB} = \begin{pmatrix} 0.1755 + 0.0000i & -0.0315 + 0.0250i & -0.0039 + 0.0480i & -0.0011 + 0.0031i \\ -0.0315 - 0.0250i & 0.3369 + 0.0000i & 0.2709 - 0.2559i & 0.0279 - 0.0128i \\ -0.0039 - 0.0480i & 0.2709 + 0.2559i & 0.4797 + 0.0000i & 0.0339 - 0.0049i \\ -0.0011 - 0.0031i & 0.0279 + 0.0128i & 0.0339 + 0.0049i & 0.0079 + 0.0000i \end{pmatrix} \quad (56)$$

This state takes into account the effect of experimental imperfections in the state preparation, such as decoherence channels, pulse shapes, and measurement errors.

With SDP (26) we compute for the 2 level displacement-based measurement the data shown in Figure 10, and for the 2 level parity-based measurement the data in Figure 11, both for 2,3 and 4 measurement settings.

Here, a `cvx_status` of 0 denotes the case where the SDP failed to find a corresponding LHS model whereas 2/3 represents an *Inaccurate/Solved* result. The latter result can be interpreted according to [CVX User's Guide](#) in a way that “[...] *the solver was unable to make a determination within the default numerical tolerance. However, it determined that the results obtained satisfied a “relaxed tolerance level”*”. Furthermore, 1/3 illustrates the *Infeasible* case, where “[...] *the problem has been proven to be infeasible through the discovery of an unbounded direction*”. For a `cvx_status` equal to 1, a solution to the SDP has been found.



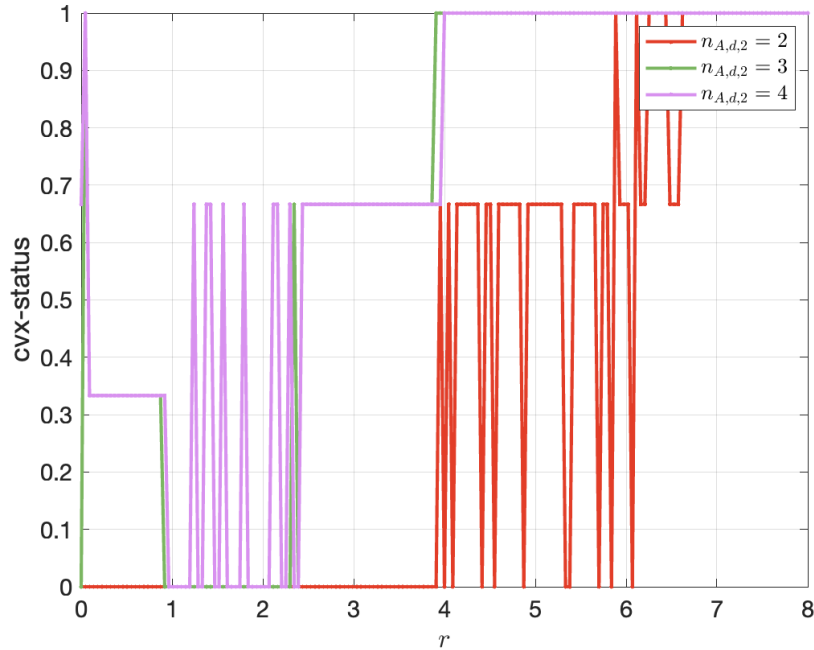


Figure 10: Plotting the `cvx-status` against  $r$  for the 2 level displacement-based measurement for 2, 3 and 4 measurement settings and the simulated density matrix  $\rho_{AB}$ . The measurement setting phases are given in Table 1. A value of 0 denotes the "Failed" case,  $1/3$  illustrates the status "Infeasible" whereas  $2/3$  stands for "Inaccurate/Solved" and 1 represents the "Solved" scenario.

Remember that if the SDP fails to find a LHS model, the considered density matrix is considered to be steerable, while in the opposite case, it will be unsteerable. Thus, one can conclude that only if `cvx-status` takes the value 1, a LHS model has truly been found and  $\rho_{AB}$  is unsteerable. For the outcome  $2/3$ , a LHS model can be found when we accept a greater numerical tolerance level, so in this case, it is a bit unclear if  $\rho_{AB}$  is steerable or not. Finally, for the outcome  $1/3$ , we can be sure that no LHS model can be created, thus the density matrix has been determined to be steerable.

From Figures 10 and 11, we can clearly see that the `cvx-status` depends on  $r$  in both scenarios.

Indeed, let us first discuss Figure 10 in greater detail. For  $n_{A,d,2} = 2$ , no true LHS model can be found until  $r$  reaches approximately 6. Upon there, it jumps from the *Inaccurate/Solved* status to the *Solved* status. Only from  $r$  greater than approximately 6.6, one can deduce that (56) is and stays unsteerable. Next, in the case of  $n_{A,d,2} = 3$  and  $n_{A,d,2} = 4$ , one notices

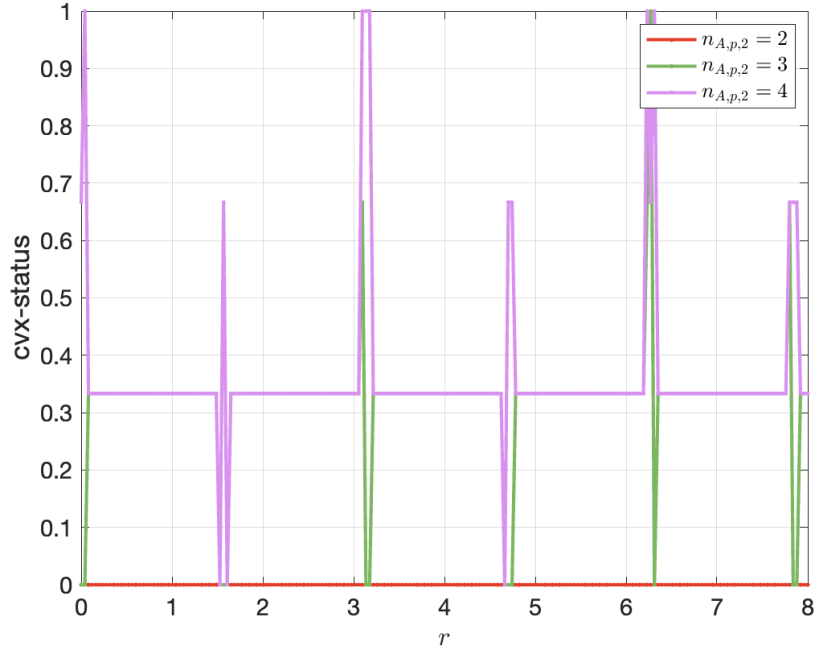


Figure 11: Plotting the cvx-status against  $r$  for the 2 level parity-based measurement for 2, 3 and 4 measurement settings and the simulated density matrix  $\rho_{AB}$ . The measurement setting phases are given in Table 1. A value of 0 denotes the "Failed" case,  $1/3$  illustrates the status "Infeasible" whereas  $2/3$  stands for "Inaccurate/Solved" and 1 represents the "Solved" scenario.

that the SDP (26) is able to find a LHS model for (56) at  $r$  being close to 0. Then, the SDP fails to find again a LHS model until  $r \approx 4$ , after which it keeps outputting the status *Solved*. Thus, a similar behaviour of the different curves can be observed. First, (56) comes out to be steerable (except for an  $r$  close to 0 for  $n_{A,d,2} = 3$  and  $n_{A,d,2} = 4$ ) up to a point, where it then switches to a permanent unsteerable setting.

Secondly, we will have a closer look at Figure 11. What stands out is that for  $n_{A,p,2} = 2$ , the SDP outputs the status "Failed" for every  $r$ , i.e. no LHS model can be found. Thus, (56) will be steerable for all  $r$  in that case. This notion is similar for  $n_{A,p,2} = 3$ . However, for  $n_{A,p,2} = 4$ , one realizes that the "steerability setting" of (56) has a periodic behaviour. Indeed, (56) becomes unsteerable with a periodic interval of about 3 units.

Thus, it can be deduced that for the density matrix (56), finding a LHS model and determining whether it is steerable respectively unsteerable is particularly dependent on  $r$ .

### 3.4 Steering inequality

#### 3.4.1 Dual SDP result

In order to obtain the steering inequalities, we will make use of the dual solution of the SDP (13). According to Ref.[17] it should be possible to obtain from this the **positive semidefinite** matrices  $F_{a|x}$ . Those  $F_{a|x}$  matrices will then allow us to define the steering inequality (16) as explained previously. Any assemblage  $\{\sigma'_{a|x}\}_{a,x}$  providing a larger value than  $S'_{max}$  is then steerable, and hence confirms that the shared state from which it was obtained is entangled.

Nevertheless, when implementing the SDP program (13) in MATLAB and trying to reproduce the results of Ref.[17], we run into the issue that the output matrices were neither positive semidefinite, nor matching the steering matrices  $G_R$  in (27) and  $G'_x$  for  $x = 1, 2, 3, 4$  in (28). Our results can be seen in section B.

To make sure that there was no potential bug or logical error in our code, we decided to rewrite it from scratch. Nevertheless, we found exactly the same results. In addition, a [GitHub link](#) was found in Ref.[26], containing code snippets about quantum steering and SDP's, which only had to be slightly adapted to match our SDP from (13). The modified code snippet depicts an additional approach computing the SDP (13) and can be found in section B. By comparing the matrices from the different procedures, so from the initial SDP and the SDP from Ref.[26], one could notice that they are very alike. Now, this was confusing, since we were still not able to reproduce (27) and (28).

In addition, we even compute analytically the dual SDP (13), which also gave us the same results. The derivation of the dual SDP as well as the corresponding results can be seen in section C.

Since we have obtained very similar results for the dual SDP by means of three independent tests and approaches, we will assume that they are correct. In fact a possibility remains, that the  $F$  positive semidefinite matrices entering a steering inequality have to be constructed from the dual SDP outputs in some nontrivial way. We did not have the time to progress along this direction during this project, but we are in touch with the authors of Ref.[17] and will look for an answer to this issue.

### 3.4.2 Steering inequalities

Assuming that our results are valid, we can now compute the SDP (16) for the different scenarios, i.e. for displacement-based measurements for a 2 level system for  $x \in \{2, 3, 4\}$  as well as for parity-based measurements for 2,3 and 4 level systems for  $x \in \{2, 3, 4\}$ . In Figures 12, 13, 14 and 15,  $S'_{max}$  is plotted against  $r$ , i.e. the "steering bound" in relation to  $r$ .

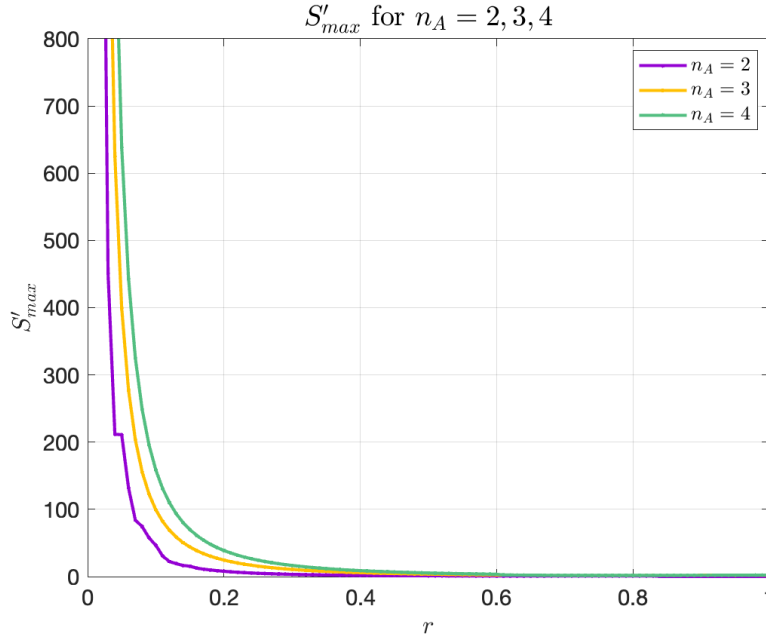


Figure 12: Plotting  $S'_{max}$  against  $r$  for the 2 level system for 2, 3 and 4 displacement-based measurement settings.

In addition, Figure 16 displays all the previous curves in order to see the individual behaviours of  $S'_{max}$  with respect to  $r$ .

As a reminder, the steering inequalities we are considering are of the form:

$$\text{Tr} \sum_{a,x} F_{a|x} \sigma'_{a|x} \leq S'_{max}. \quad (57)$$

Any assemblage  $\{\sigma'_{a|x}\}_{a,x}$  that is providing a larger value than  $S'_{max}$ , i.e. leads to a violation of the above equation, is steerable, and hence confirms that the shared state is indeed entangled.

Taking a closer look at Figures 12, 13, 14 and 15, one notices how the steerability bound  $S'_{max}$  depends on  $r$ . Indeed, from Figure 12,  $S'_{max}$  seems to be declining exponentially with  $r$  for the

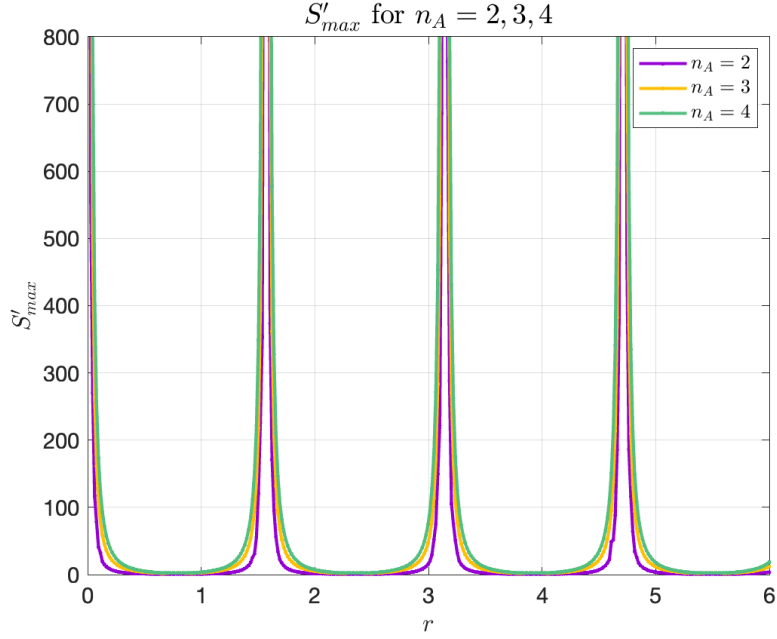


Figure 13: Plotting  $S'_{max}$  against  $r$  for the 2 level system for 2, 3 and 4 parity-based measurement settings.

2 level displacement measurements and tends to go to 0. However, we cannot find a physical interpretation for this, since we have lost the positive semidefinite constraint regarding the  $F_{a|x}$  matrices. Furthermore, for the parity measurements, one can also recognize in Figures 13, 14 and 15 how  $S'_{max}$  oscillates with respect to  $r$  and illustrate the same periodic pattern we initially found when investigating the behaviour of  $\eta_*$ .

In the future, it would be interesting to find a steering inequality based on Wigner functions, similarly to the Bell-type inequality found in Ref.[27],[28]. These ideas are sketched in section D.

## 4 Conclusion

During this project, we looked at the EPR steering phenomenon for displacement and parity-based detection in multiple levels systems. In a first part, we searched for the critical value of the detection efficiency and discovered that the value of  $\eta_*$  increases differently with respect to  $r$  for different number of measurement settings. We came across the notion that when looking at parity-based measurements, we were able to observe some periodic behaviours. This was

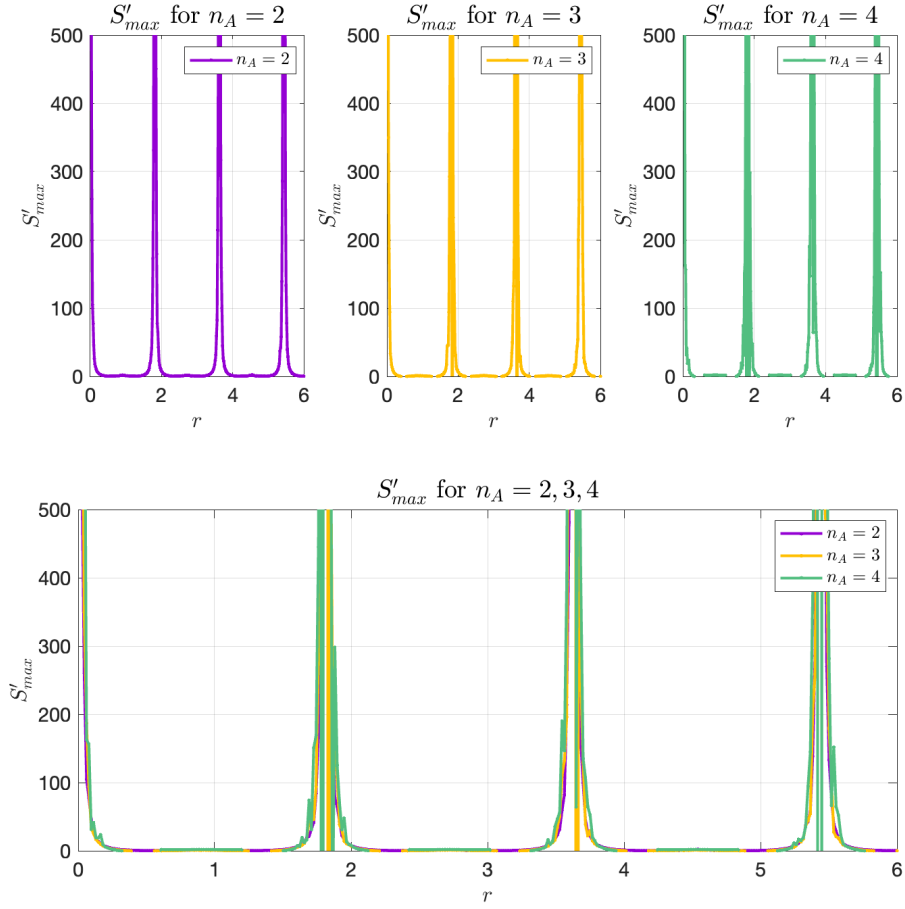


Figure 14: Plotting  $S'_{max}$  against  $r$  for the 3 level system for 2, 3 and 4 parity-based measurement settings.

in accordance with the results we acquired with the inspection of  $S'_{max}$ . Unfortunately, we need to make the remark that we encountered an issue during the analysis of this project. Indeed, we were unable to reproduce the correct form of the steering functionals as given in Ref.[17]. In order to check for this, we employed different techniques and procedures in order to find possible mistakes or logical errors in our analysis. However, this seemed not to be the case, as we found very similar results from independent method. Therefore, we assumed that our initial approach was valid. Finally, we obtained a simulated density matrix for 2 entangled qubits with realistic experimental parameters and imperfections. Here, we came upon the idea that when considering displacement-based measurements, the simulated

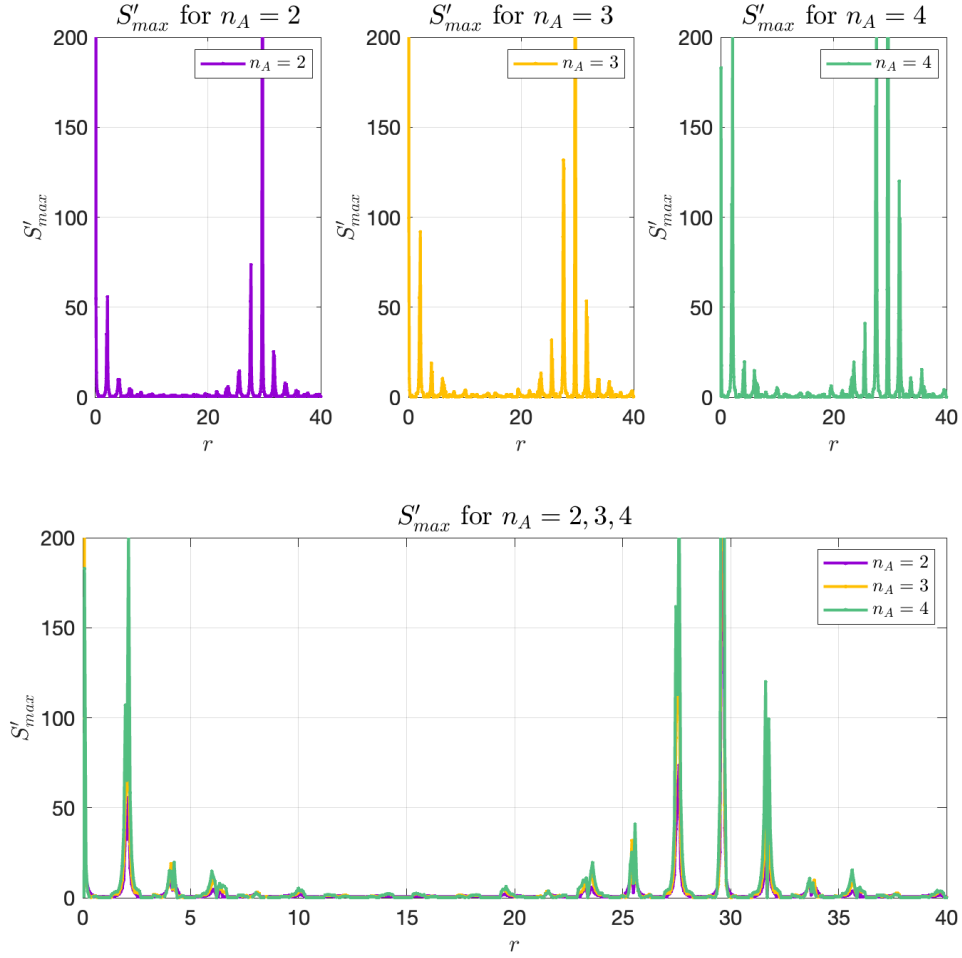


Figure 15: Plotting  $S'_{max}$  against  $r$  for the 4 level system for 2, 3 and 4 parity-based measurement settings.

density matrix can be seen to be steerable for small  $r$ , up to a critical value of  $r$  that does not allow to detect steering anymore. This was unlike the case where we looked at parity-based measurements. Indeed, for 2 and 3 measurement settings, the simulated density matrix came out to be steerable for all  $r$ .

In the future, our result could be useful to detect EPR steering between pairs of systems based on parity measurements. Examples include Wigner-function measurements on entangled mechanical oscillators, such as in the experiment performed by the group of Prof. Y. Chu.

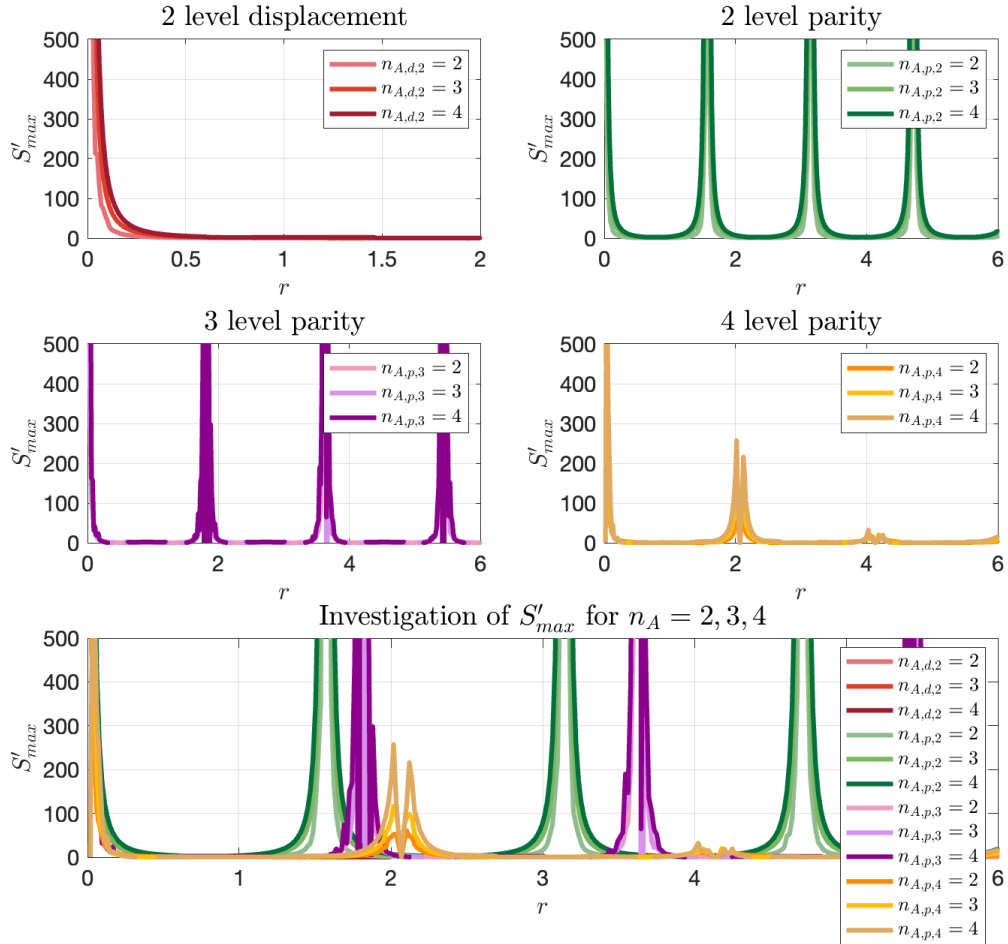


Figure 16: Combined curves from Figures 12, 13, 14, 15 in the range  $r \in [0, 6]$  and  $S'_{max} \in [0, 500]$ . Here,  $n_{A,d,i}$  describes the number of measurement settings for the displacement-based measurement and the  $i$  level, while  $n_{A,p,i}$  represents the number of measurement settings for the parity-based measurement and the  $i$  level.



### **Acknowledgement**

Many thanks to Dr. Matteo Fadel. I had the pleasure of being supervised by him and he was always ready to help me with any questions and guided me throughout this intriguing project.

## A Definitions and calculation steps

This section revisits various definitions and derivations, some of which may be important for understanding the individual calculation steps.

▷ The representation of the coherent state  $|\alpha\rangle$  in the Fock basis [29] is given by

$$|\alpha\rangle = e^{-\frac{|\alpha|^2}{2}} \sum_{n=0}^{\infty} \frac{\alpha^n}{\sqrt{n!}} |n\rangle. \quad (58)$$

So computing the projector in (17) gives:

$$\Pi(\alpha) = e^{-|\alpha|^2} \sum_{n,m=0}^{\infty} \frac{\alpha^n (\alpha^*)^m}{\sqrt{n!m!}} |n\rangle\langle m|. \quad (59)$$

Hence, restricting the Hilbert space to two levels we have

$$\Pi(\alpha) = \begin{pmatrix} e^{-r^2} & r e^{-r^2-i\theta} \\ r e^{-r^2+i\theta} & r^2 e^{-r^2} \end{pmatrix}. \quad (60)$$

▷ We seek to find the matrix representation of the creation operator  $\hat{a}^\dagger$  for the 1-dimensional harmonic oscillator. Remember that for an energy eigenstate  $|n\rangle$ , we have:

$$\hat{a}^\dagger |n\rangle = \sqrt{n+1} |n+1\rangle. \quad (61)$$

Computing the matrix elements gives

$$\hat{a}_{ij}^\dagger = \langle i | \hat{a}^\dagger | j \rangle = \sqrt{j+1} \delta_{i(j+1)}, \quad (62)$$

and therefore

$$\hat{a}^\dagger = \begin{pmatrix} 0 & 0 & 0 & 0 & \dots \\ \sqrt{1} & 0 & 0 & 0 & \dots \\ 0 & \sqrt{2} & 0 & 0 & \dots \\ 0 & 0 & \sqrt{3} & 0 & \dots \\ 0 & 0 & 0 & \sqrt{4} & \dots \\ \dots & \dots & \dots & \dots & \dots \end{pmatrix}, \quad (63)$$

as well as

$$\hat{a} = \begin{pmatrix} 0 & \sqrt{1} & 0 & 0 & 0 & \dots \\ 0 & 0 & \sqrt{2} & 0 & 0 & \dots \\ 0 & 0 & 0 & \sqrt{3} & 0 & \dots \\ 0 & 0 & 0 & 0 & \sqrt{4} & \dots \\ \dots & \dots & \dots & \dots & \dots & \dots \end{pmatrix}. \quad (64)$$

▷ We can split the exponential series from (31) into terms of even and odd powers in  $X$ :

$$\exp(X) = \sum_{k=0}^{\infty} \frac{X^{2k}}{(2k)!} + \sum_{k=0}^{\infty} \frac{X^{2k+1}}{(2k+1)!}. \quad (65)$$

Substituting (32) and (33) into (65) then states:

$$\begin{aligned} \exp(X) &= \sum_{k=0}^{\infty} \frac{(-1)^k (\sqrt{\alpha^* \alpha})^{2k}}{(2k)!} \mathbb{1} - \sum_{k=0}^{\infty} \frac{(-1)^k (\sqrt{\alpha^* \alpha})^{2k}}{(2k+1)!} X \\ &= \cos(\sqrt{\alpha^* \alpha}) \mathbb{1} - \sum_{k=0}^{\infty} \frac{(-1)^k (\sqrt{\alpha^* \alpha})^{2k+1}}{(2k+1)! \sqrt{\alpha^* \alpha}} X \\ &= \cos(\sqrt{\alpha^* \alpha}) \mathbb{1} - \frac{1}{\sqrt{\alpha^* \alpha}} \sin(\sqrt{\alpha^* \alpha}) X. \end{aligned}$$

With  $\alpha = \exp(re^{i\theta})$ , we note that  $\sqrt{\alpha^* \alpha} = \sqrt{r^2} = r$ , since  $r \geq 0$  in our case. With this, we finally obtain (34).

▷ The state (4) for 2, 3 and 4 levels is explicitly given by the following matrices:

$$\begin{aligned} |\Psi\rangle_2 &= \frac{1}{\sqrt{2}} \begin{pmatrix} 0 & 1 & 1 & 0 \end{pmatrix}^\top, \\ |\Psi\rangle_3 &= \frac{1}{\sqrt{2}} \begin{pmatrix} 0 & 1 & 0 & 1 & 0 & 0 & 0 & 0 \end{pmatrix}^\top, \\ |\Psi\rangle_4 &= \frac{1}{\sqrt{2}} \begin{pmatrix} 0 & 1 & 0 & 0 & 1 & 0 & 0 & 0 & 0 & 0 & 0 & 0 \end{pmatrix}^\top. \end{aligned}$$

▷ Let  $A$  and  $B$  represent the two subsystems that make up the composite system defined by the density operator  $\rho_{AB}$ . A generic two-qubit state  $\rho_{AB}$  can be expanded with respect

to the orthonormal basis  $\{|0, 0\rangle, |0, 1\rangle, |1, 0\rangle, |1, 1\rangle\}$  as:

$$\rho_{AB} = \rho_{11} |0, 0\rangle\langle 0, 0| + \rho_{12} |0, 0\rangle\langle 0, 1| + \cdots + \rho_{44} |1, 1\rangle\langle 1, 1|. \quad (66)$$

Then, the partial trace over the subsystem  $A$ , given by  $\text{Tr}_A$ , is specified by the expression:

$$\text{Tr}_A[\rho_{AB}] := \sum_i (\langle i|_A \otimes \mathbb{1}_B) \rho_{AB} (|i\rangle_A \otimes \mathbb{1}_B), \quad (67)$$

where  $|i\rangle$  represents any orthonormal basis for the Hilbert space  $\mathcal{H}_A$  of the subsystem  $A$  [30].

For convenience we state the formula for two qubits [31]:

$$\text{Tr}_A[\rho_{AB}] = \begin{pmatrix} \rho_{11} & \rho_{12} & \rho_{13} & \rho_{14} \\ \rho_{21} & \rho_{22} & \rho_{23} & \rho_{24} \\ \rho_{31} & \rho_{32} & \rho_{33} & \rho_{34} \\ \rho_{41} & \rho_{42} & \rho_{43} & \rho_{44} \end{pmatrix} \quad (68)$$

$$= \begin{pmatrix} \rho_{11} + \rho_{33} & \rho_{12} + \rho_{34} \\ \rho_{21} + \rho_{43} & \rho_{22} + \rho_{44} \end{pmatrix}. \quad (69)$$

## B SDP

In this section, we present the results for the  $F$  and  $G$  matrices for the different methods of the SDP, so for our initial SDP program and the modified SDP code from Ref.[26]. Consequently, we can get a sense whether we have a bug in our initial code or if we can assume that it outputs valid results. In addition, we consider another approach for this, which will be explained in section C.

The following outputs are for  $r = 0.2$  and the 4 measurement settings  $\theta_1 = 0$ ,  $\theta_2 = \pi/2$ ,  $\theta_3 = \pi$  and  $\theta_4 = 3\pi/2$  considering displacement measurements for a 2 level system.

```

1
2 % First Draft of SDP
3
4 % results of F_{a|x}: + is given by p, - is given by m, x=1,2,3 or 4
5
6 Fp1 =
7
8   -0.4196 + 0.0000i    2.0562 - 0.0000i
9     2.0562 + 0.0000i   -30.2315 + 0.0000i
10
11 Fm1 =
12
13   -0.4196 + 0.0000i   -0.0000 - 0.0000i
14   -0.0000 + 0.0000i  -40.3082 + 0.0000i
15
16 Fp2 =
17
18    0.0000 + 0.0000i    0.0000 - 2.0562i
19    0.0000 + 2.0562i   10.0772 + 0.0000i
20
21 Fm2 =
22
23    1.0e-03 *
24
25   -0.0000 + 0.0000i    0.0000 - 0.0000i
26    0.0000 + 0.0000i    0.4885 + 0.0000i
27
28 Fp3 =
29
30   -0.0000 + 0.0000i   -2.0562 + 0.0000i
31   -2.0562 - 0.0000i   10.0772 + 0.0000i
32
33 Fm3 =

```

```
34
35     1.0e-03 *
36
37     -0.0000 + 0.0000i   -0.0000 + 0.0000i
38     -0.0000 - 0.0000i    0.4885 + 0.0000i
39
40 Fp4 =
41
42     -0.0000 + 0.0000i    0.0000 + 2.0562i
43     0.0000 - 2.0562i   10.0772 + 0.0000i
44
45 Fm4 =
46
47     1.0e-03 *
48
49     -0.0000 + 0.0000i    0.0000 + 0.0000i
50     0.0000 - 0.0000i    0.4885 + 0.0000i
51
52
53 % results of the steering matrices GRprime and Gxprime
54
55 GRprime =
56
57     -0.4196 + 0.0000i   -0.0000 - 0.0000i
58     -0.0000 + 0.0000i  -40.3067 + 0.0000i
59
60 Gxprime1 =
61
62     0.0000 + 0.0000i    2.0562 + 0.0000i
63     2.0562 - 0.0000i   10.0767 + 0.0000i
64
65 Gxprime2 =
66
67     0.0000 + 0.0000i    0.0000 - 2.0562i
68     0.0000 + 2.0562i   10.0767 + 0.0000i
69
70 Gxprime3 =
71
72     0.0000 + 0.0000i   -2.0562 + 0.0000i
73     -2.0562 - 0.0000i  10.0767 + 0.0000i
74
75 Gxprime4 =
76
77     0.0000 + 0.0000i    0.0000 + 2.0562i
```

```

78      0.0000 - 2.0562i  10.0767 + 0.0000i
1
2 % Second Draft of SDP
3
4 % results of F_{a|x}: + is given by p, - is given by m, x=1,2,3 or 4
5
6 Fp1 =
7
8      -0.4196 + 0.0000i   2.0566 - 0.0000i
9      2.0566 + 0.0000i  -30.2432 + 0.0000i
10
11 Fm1 =
12
13      -0.4196 + 0.0000i   -0.0000 - 0.0000i
14      -0.0000 + 0.0000i  -40.3242 + 0.0000i
15
16 Fp2 =
17
18      0.0000 + 0.0000i   -0.0000 - 2.0566i
19      -0.0000 + 2.0566i  10.0811 + 0.0000i
20
21 Fm2 =
22
23      1.0e-10 *
24
25      -0.1114 + 0.0000i   0.0007 - 0.0033i
26      0.0007 + 0.0033i   -0.0153 + 0.0000i
27
28 Fp3 =
29
30      0.0000 + 0.0000i   -2.0566 - 0.0000i
31      -2.0566 + 0.0000i  10.0811 + 0.0000i
32
33 Fm3 =
34
35      1.0e-10 *
36
37      -0.3022 + 0.0000i   0.0043 - 0.0003i
38      0.0043 + 0.0003i   -0.0386 + 0.0000i
39
40 Fp4 =
41
42      0.0000 + 0.0000i   0.0000 + 2.0566i

```

```

43     0.0000 - 2.0566i  10.0811 + 0.0000i
44
45 Fm4 =
46
47     1.0e-10 *
48
49     -0.2203 + 0.0000i    0.0048 + 0.0045i
50     0.0048 - 0.0045i   -0.0597 + 0.0000i
51
52 % results of the steering matrices GRprime and Gxprime
53
54 GRprime =
55
56     -0.4196 + 0.0000i   -0.0000 - 0.0000i
57     -0.0000 + 0.0000i  -40.3242 + 0.0000i
58
59 Gxprime1 =
60
61     0.0000 + 0.0000i    2.0566 - 0.0000i
62     2.0566 + 0.0000i   10.0811 + 0.0000i
63
64 Gxprime2 =
65
66     0.0000 + 0.0000i   -0.0000 - 2.0566i
67     -0.0000 + 2.0566i   10.0811 + 0.0000i
68
69 Gxprime3 =
70
71     0.0000 + 0.0000i   -2.0566 - 0.0000i
72     -2.0566 + 0.0000i   10.0811 + 0.0000i
73
74 Gxprime4 =
75
76     0.0000 + 0.0000i   -0.0000 + 2.0566i
77     -0.0000 - 2.0566i   10.0811 + 0.0000i

```

One can notice that the matrices for the 2 strategies are very similar, are not positive semidefinite and do not match with (27) and (28).

The code snippets for the different SDP methods are presented in the following.

```

1
2 % First SDP approach
3

```



```

4 cvx_begin SDP quiet
5 cvx_solver SeDuMi %mosek
6 cvx_precision best
7
8     variables p                               % defines eta
9     variable sigmaL(dB*Ndet,dB) complex      % vector containing the sigma_B(a|x
10 )
11 dual variables F{Ndet,dB}
12 dual variable K{1,1}
13
14 maximise( p )
15
16 % the following computes the sum of D_lambda(a,x)*sigma_lambda over all
17 lambda, and asks it to be equal to the assemblage
18 % further we solve the dual problem where F is a 2x2 matrix
19 subject to
20
21 p >= 0;
22 p <= 1;
23
24 % sig_a|x == \sum_lam D(a|x,lam) sigmaL
25 for i = 1:mA*nA
26     F{i} : Tensor(SingleParty(i,:),IddB)*sigmaL == p * assemblageS(1+(i
27 -1)*dB:i*dB,:) + (1-p) * assemblageUS(1+(i-1)*dB:i*dB,:);
28 end
29
30 % ask every sigmaL to be positive semidefinite
31 for i = 1:Ndet
32     sigmaL(1+(i-1)*dB:i*dB,:) == hermitian_semidefinite(dB);
33 end
34
35 % sum_lam tr(sigmaL) == 1
36 sum = zeros(dB,dB);
37 for i = 1:Ndet
38     sum = (sum + sigmaL(1+(i-1)*dB:i*dB,:));
39 end
40 K{1} : trace(sum) == 1;
41
42 cvx_end
43
44 % Second SDP approach (modified version from GitHub)

```

```
45 cvx_begin sdp quiet
46 cvx_solver SeDuMi
47
48     variable p           % defines eta
49     variable siglam(dB,dB,Ndet) hermitian semidefinite % siglam are the
members of the LHS model
50     dual variable F
51
52     maximise( p )
53
54     subject to
55
56     p >= 0;
57     p <= 1;
58
59     % sig_a|x == \sum_lam D(a|x,lam) sig_lam
60     F : p*sigmaS + (1-p)*sigmaUS == squeeze(sum(repmat(siglam,[1,1,1,mA,nA])
...
61         .*permute(repmat(SingleParty,[1,1,1,dB,dB]],[4,5,3,1,2]),3));
62
63     % ensures normalisation
64     trace(sum(siglam,3)) == 1;
65
66 cvx_end
```

## C Dual SDP

In this section, we will present our procedure to analytically derive the dual SDP problem to the SDP (13) in the case of 4 measurement settings.

### C.1 Duality theory

Analogously to linear programming, given a general SDP of the form<sup>6</sup>

$$\min_{X \in \mathbb{S}^n} \langle C, X \rangle_{\mathbb{S}^n} \quad (70)$$

$$\text{subject to } \langle A_i, X \rangle_{\mathbb{S}^n} = b_i \quad i = 1, \dots, m \quad (71)$$

$$X \geq 0, \quad (72)$$

(the primal problem or P-SDP), we define the *dual* semidefinite program (D-SDP) as

$$\max_{y \in \mathbb{R}^m} \langle b, y \rangle_{\mathbb{R}^m} \quad (73)$$

$$\text{subject to } \sum_{i=1}^m y_i A_i \leq C, \quad (74)$$

where for any two matrices  $P$  and  $Q$ ,  $P \leq Q$  means  $P - Q \leq 0$  [22].

### C.2 Derivation

Our goal now is to solve the P-SDP and D-SDP on the following problem:

$$\eta_* \equiv \max_{\eta} \eta \quad 0 \leq \eta \leq 1 \quad (75)$$

$$\text{subject to } \sum_{\lambda} D_{\lambda}(a|x) \sigma_{\lambda} = \eta \sigma_{a|x}^S(\eta) + (1 - \eta) \sigma_{a|x}^{US}(\eta) \quad \forall a, x \quad (76)$$

$$\text{Tr} \sum_{\lambda} \sigma_{\lambda} = 1, \quad \sigma_{\lambda} \geq 0. \quad (77)$$

#### C.2.1 Primal

For the P-SDP, we first define the corresponding matrices for our problem<sup>7</sup>.

We have:

---

<sup>6</sup>Remark: remember that  $\langle A, X \rangle = \text{Tr}(A \cdot X^{\dagger})$ .

<sup>7</sup>Note:  $X, A_0, A_{\text{tr}}, A_{a|x}$  and  $C$  are 34x34 matrices in this specific case of 4 measurement settings.

$$X = \begin{pmatrix} \sigma_{0000} & & & & \\ & \sigma_{0001} & & & \\ & & \ddots & & \\ & & & \sigma_{1111} & \\ & & & & x \\ & & & & & y \end{pmatrix}, \quad (78)$$

where  $\sigma_\lambda$  represent hermitian 2x2 matrices with  $\lambda = (0000, 0001, \dots, 1111)$ ,  $x = \eta$  and  $y = (1 - \eta)$ . One immediately sees that  $X \geq 0$ .

Next,

$$C = \begin{pmatrix} 0 & & & & \\ & 0 & & & \\ & & \ddots & & \\ & & & 0 & \\ & & & & -1 \\ & & & & & 0 \end{pmatrix}. \quad (79)$$

Those definitions of the matrices make sense since  $\max f = -\min(-f)$  for a function  $f$ . Then,  $\min\langle C, X \rangle = -\max x = -\max \eta$ , which in fact describes the maximisation problem in equation (75).

Now, we consider the constraints that  $0 \leq \eta \leq 1$  and that  $\text{Tr}\sum_\lambda \sigma_\lambda = 1$ .

- $0 \leq \eta \leq 1$ :

We define:

$$A_0 = \begin{pmatrix} 0 & & & & \\ & 0 & & & \\ & & \ddots & & \\ & & & 0 & \\ & & & & 1 \\ & & & & & 1 \end{pmatrix}, \quad (80)$$

such that  $\langle A_0, X \rangle = x + y = \eta + 1 - \eta = 1 \equiv b_0$ .



The  $D_{0000}(a|x), \dots, D_{1111}(a|x)$  denote the deterministic response function defined by  $D_\lambda(a|x) = \delta_{a,\lambda(x)}$ , where  $\lambda(x)$  denotes the value of the outcome at position  $x$ . This means that  $D_\lambda(a|x)$  equals one for strings  $\lambda$  which predict the outcome  $a$  for the measurement  $x$  and zero otherwise [8].

With the definition of  $(A_{a|x})^{i,j}$ , we thus have:

$$\begin{aligned} \langle (A_{a|x})^{i,j}, X \rangle &= D_{0000}(a|x) \cdot (\sigma_{0000}^{ij} \delta_{ij} + \sigma_{0000}^{i(j-1)} \delta_{i(j-1)}) + D_{0000}(a|x) \cdot (\sigma_{0000}^{(i-1)j} \delta_{(i-1)j} \\ &\quad + \sigma_{0000}^{(i-1)(j-1)} \delta_{(i-1)(j-1)}) + D_{1111}(a|x) \cdot (\sigma_{1111}^{ij} \delta_{ij} + \sigma_{1111}^{i(j-1)} \delta_{i(j-1)}) \\ &\quad + D_{1111}(a|x) \cdot (\sigma_{1111}^{(i-1)j} \delta_{(i-1)j} + \sigma_{1111}^{(i-1)(j-1)} \delta_{(i-1)(j-1)}) - x(\sigma_{a|x}^S)^{i,j} - y(\sigma_{a|x}^{US})^{i,j}. \end{aligned}$$

This matches with the expression (82).

To sum up, we now have the following P-SDP, expressed in the form of (70):

$$\min \quad \langle C, X \rangle \quad (84)$$

$$\text{subject to} \quad \langle A_0, X \rangle = b_0 \quad (85)$$

$$\langle A_{\text{tr}}, X \rangle = b_{\text{tr}} \quad (86)$$

$$\langle (A_{a|x})^{i,j}, X \rangle = (b_{a|x})^{i,j} \quad \forall a, x \quad i, j \in \{1, 2\}. \quad (87)$$

### C.2.2 Dual

To solve the dual problem, we introduce the 34-dimensional vectors:

$$b = \begin{pmatrix} (b_{+1|1})^{1,1} \\ (b_{+1|1})^{1,2} \\ (b_{+1|1})^{2,1} \\ (b_{+1|1})^{2,2} \\ \vdots \\ (b_{-1|4})^{2,2} \\ b_0 \\ b_{\text{tr}} \end{pmatrix}, \quad y = \begin{pmatrix} (y_{+1|1})^{1,1} \\ (y_{+1|1})^{1,2} \\ (y_{+1|1})^{2,1} \\ (y_{+1|1})^{2,2} \\ \vdots \\ (y_{-1|4})^{2,2} \\ y_0 \\ y_{\text{tr}} \end{pmatrix},$$

where each entry of the  $y$  vector illustrates a specific dual variable. In our case, the dual variables  $y_{a|x}$  for  $a \in \{+1, -1\}$ ,  $x \in \{1, 2, 3, 4\}$  will represent the 2x2  $F_{a|x}$  matrices from

Ref.[17] and  $y_0$  and  $y_{\text{tr}}$  are the corresponding dual scalars of  $b_0$  and  $b_{\text{tr}}$ .

From equation (73), we notice that we seek to maximise  $\langle b, y \rangle = y_0 + y_{\text{tr}}$ .

Similar to the subsection above, we will now consider the constraint from equation (74):

$$\sum_{k=1}^{34} y_k A_k - C \leq 0. \quad (88)$$

We will separate some individual steps for a better overview.

For  $k = 1, \dots, 8$ :

$$\left( \begin{array}{cccc} D_{0000}(a|x) \cdot \sum_{a,x} y_{a|x} & & & \\ & \ddots & & \\ & & D_{1111}(a|x) \cdot \sum_{a,x} y_{a|x} & \\ & & & - \sum_{a,x,i,j} (\sigma_{a|x}^S)^{i,j} \cdot y_{a|x}^{i,j} \\ & & & - \sum_{a,x,i,j} (\sigma_{a|x}^{US})^{i,j} \cdot y_{a|x}^{i,j} \end{array} \right).$$

For  $k = 9, \dots, 10$ :

$$\left( \begin{array}{cccc} y_{\text{tr}} & & & \\ & y_{\text{tr}} & & \\ & & \ddots & \\ & & & y_{\text{tr}} \\ & & & & y_0 \\ & & & & & y_0 \end{array} \right).$$

Thus we get the constraint:

$$\left( \begin{array}{cccc} D_{0000}(a|x) \cdot \sum_{a,x} y_{a|x} + y_{\text{tr}} \cdot \mathbb{I}_2 & & & \\ & \ddots & & \\ & & D_{1111}(a|x) \cdot \sum_{a,x} y_{a|x} + y_{\text{tr}} \cdot \mathbb{I}_2 & \\ & & & y_0 + 1 - \sum_{a,x,i,j} (\sigma_{a|x}^S)^{i,j} \cdot (y_{a|x})^{i,j} \\ & & & & y_0 - \sum_{a,x,i,j} (\sigma_{a|x}^{US})^{i,j} \cdot (y_{a|x})^{i,j} \end{array} \right) \leq 0,$$

where

$$y_{a|x} := \begin{pmatrix} y_{a|x}^{1,1} & y_{a|x}^{1,2} \\ y_{a|x}^{2,1} & y_{a|x}^{2,2} \end{pmatrix}.$$

To sum up, we now have the following D-SDP:

$$\max_{y \in \mathbb{R}^m} \langle b, y \rangle_{\mathbb{R}^m} \quad (89)$$

$$\text{subject to } y_{\text{tr}} \cdot \mathbb{I}_2 + \sum_{a,x} D_\lambda(a|x) \cdot y_{a|x} \leq 0 \quad \forall \lambda \quad (90)$$

$$y_0 + 1 - \sum_{a,x} \text{Tr}[\sigma_{a|x}^S \cdot y_{a|x}] \leq 0 \quad (91)$$

$$y_0 - \sum_{a,x} \text{Tr}[\sigma_{a|x}^{US} \cdot y_{a|x}] \leq 0 \quad (92)$$

Respectively:

$$\max_{y \in \mathbb{R}^m} \langle b, y \rangle_{\mathbb{R}^m} \quad (93)$$

$$\text{subject to } -y_{\text{tr}} \cdot \mathbb{I}_2 - \sum_{a,x} D_\lambda(a|x) \cdot y_{a|x} \geq 0 \quad \forall \lambda \quad (94)$$

$$-y_0 - 1 + \sum_{a,x} \text{Tr}[\sigma_{a|x}^S \cdot y_{a|x}] \geq 0 \quad (95)$$

$$-y_0 + \sum_{a,x} \text{Tr}[\sigma_{a|x}^{US} \cdot y_{a|x}] \geq 0 \quad (96)$$

## C.3 Calculation

### C.3.1 Primal

For the primal part, I am quite confident that the acquired values seem fine, so we will jump straight to the dual problem. MATLAB gives us the following values for  $x$  and  $y$  for  $r = 0.2$  and 4 measurement settings for the 2 level case and displacement-based measurements:

$$\begin{aligned} x &= \eta = 0.4196, \\ y &= 1 - \eta = 0.5804. \end{aligned}$$

### C.3.2 Dual

We seek to maximize  $\langle b, y \rangle = y_0 + y_{\text{tr}}$ .

We will go over the constraints in detail. Remembering that  $D_\lambda(a|x) = \delta_{a,\lambda(x)}$ , we get for



example:

$$\begin{aligned} \sum_{a,x} D_{0000}(a|x)y_{a|x} &= 0 \cdot y_{1|1} + 0 \cdot y_{1|2} + 0 \cdot y_{1|3} + 0 \cdot y_{1|4} + 1 \cdot y_{-1|1} + 1 \cdot y_{-1|2} \\ &\quad + 1 \cdot y_{-1|3} + 1 \cdot y_{-1|4} \end{aligned}$$

Thus, we obtain:

$$\begin{aligned} -y_{\text{tr}} \cdot \mathbb{I}_2 - \sum_{a,x} D_{0000}(a|x)y_{a|x} &= -y_{\text{tr}} \cdot \mathbb{I}_2 - (1 \cdot y_{-1|1} + 1 \cdot y_{-1|2} + 1 \cdot y_{-1|3} + 1 \cdot y_{-1|4}) \geq 0 \\ -y_{\text{tr}} \cdot \mathbb{I}_2 - \sum_{a,x} D_{0001}(a|x)y_{a|x} &= -y_{\text{tr}} \cdot \mathbb{I}_2 - (1 \cdot y_{1|4} + 1 \cdot y_{-1|1} + 1 \cdot y_{-1|2} + 1 \cdot y_{-1|3}) \geq 0 \\ -y_{\text{tr}} \cdot \mathbb{I}_2 - \sum_{a,x} D_{0010}(a|x)y_{a|x} &= -y_{\text{tr}} \cdot \mathbb{I}_2 - (1 \cdot y_{1|3} + 1 \cdot y_{-1|1} + 1 \cdot y_{-1|2} + 1 \cdot y_{-1|4}) \geq 0 \\ -y_{\text{tr}} \cdot \mathbb{I}_2 - \sum_{a,x} D_{0011}(a|x)y_{a|x} &= -y_{\text{tr}} \cdot \mathbb{I}_2 - (1 \cdot y_{1|3} + 1 \cdot y_{1|4} + 1 \cdot y_{-1|1} + 1 \cdot y_{-1|2}) \geq 0 \\ -y_{\text{tr}} \cdot \mathbb{I}_2 - \sum_{a,x} D_{0100}(a|x)y_{a|x} &= -y_{\text{tr}} \cdot \mathbb{I}_2 - (1 \cdot y_{1|2} + 1 \cdot y_{-1|1} + 1 \cdot y_{-1|3} + 1 \cdot y_{-1|4}) \geq 0 \\ -y_{\text{tr}} \cdot \mathbb{I}_2 - \sum_{a,x} D_{0101}(a|x)y_{a|x} &= -y_{\text{tr}} \cdot \mathbb{I}_2 - (1 \cdot y_{1|2} + 1 \cdot y_{1|4} + 1 \cdot y_{-1|1} + 1 \cdot y_{-1|3}) \geq 0 \\ -y_{\text{tr}} \cdot \mathbb{I}_2 - \sum_{a,x} D_{0110}(a|x)y_{a|x} &= -y_{\text{tr}} \cdot \mathbb{I}_2 - (1 \cdot y_{1|2} + 1 \cdot y_{1|3} + 1 \cdot y_{-1|1} + 1 \cdot y_{-1|4}) \geq 0 \\ -y_{\text{tr}} \cdot \mathbb{I}_2 - \sum_{a,x} D_{0111}(a|x)y_{a|x} &= -y_{\text{tr}} \cdot \mathbb{I}_2 - (1 \cdot y_{1|2} + 1 \cdot y_{1|3} + 1 \cdot y_{1|4} + 1 \cdot y_{-1|1}) \geq 0 \\ -y_{\text{tr}} \cdot \mathbb{I}_2 - \sum_{a,x} D_{1000}(a|x)y_{a|x} &= -y_{\text{tr}} \cdot \mathbb{I}_2 - (1 \cdot y_{1|1} + 1 \cdot y_{-1|2} + 1 \cdot y_{-1|3} + 1 \cdot y_{-1|4}) \geq 0 \\ -y_{\text{tr}} \cdot \mathbb{I}_2 - \sum_{a,x} D_{1001}(a|x)y_{a|x} &= -y_{\text{tr}} \cdot \mathbb{I}_2 - (1 \cdot y_{1|1} + 1 \cdot y_{1|4} + 1 \cdot y_{-1|2} + 1 \cdot y_{-1|3}) \geq 0 \\ -y_{\text{tr}} \cdot \mathbb{I}_2 - \sum_{a,x} D_{1010}(a|x)y_{a|x} &= -y_{\text{tr}} \cdot \mathbb{I}_2 - (1 \cdot y_{1|1} + 1 \cdot y_{1|3} + 1 \cdot y_{-1|2} + 1 \cdot y_{-1|4}) \geq 0 \\ -y_{\text{tr}} \cdot \mathbb{I}_2 - \sum_{a,x} D_{1011}(a|x)y_{a|x} &= -y_{\text{tr}} \cdot \mathbb{I}_2 - (1 \cdot y_{1|1} + 1 \cdot y_{1|3} + 1 \cdot y_{1|4} + 1 \cdot y_{-1|2}) \geq 0 \\ -y_{\text{tr}} \cdot \mathbb{I}_2 - \sum_{a,x} D_{1100}(a|x)y_{a|x} &= -y_{\text{tr}} \cdot \mathbb{I}_2 - (1 \cdot y_{1|1} + 1 \cdot y_{1|2} + 1 \cdot y_{-1|3} + 1 \cdot y_{-1|4}) \geq 0 \\ -y_{\text{tr}} \cdot \mathbb{I}_2 - \sum_{a,x} D_{1101}(a|x)y_{a|x} &= -y_{\text{tr}} \cdot \mathbb{I}_2 - (1 \cdot y_{1|1} + 1 \cdot y_{1|2} + 1 \cdot y_{1|4} + 1 \cdot y_{-1|3}) \geq 0 \\ -y_{\text{tr}} \cdot \mathbb{I}_2 - \sum_{a,x} D_{1110}(a|x)y_{a|x} &= -y_{\text{tr}} \cdot \mathbb{I}_2 - (1 \cdot y_{1|1} + 1 \cdot y_{1|2} + 1 \cdot y_{1|3} + 1 \cdot y_{-1|4}) \geq 0 \end{aligned}$$

$$-y_{\text{tr}} \cdot \mathbb{I}_2 - \sum_{a,x} D_{1111}(a|x)y_{a|x} = -y_{\text{tr}} \cdot \mathbb{I}_2 - (1 \cdot y_{1|1} + 1 \cdot y_{1|2} + 1 \cdot y_{1|3} + 1 \cdot y_{1|4}) \geq 0.$$

For the second constraint, we will first present the values of the matrices<sup>8</sup>  $\sigma^S$  and  $\sigma^{US}$ :

$$\sigma^S = \begin{pmatrix} 0.0192 + 0.0000i & 0.0961 + 0.0000i \\ 0.0961 + 0.0000i & 0.4804 + 0.0000i \\ 0.4808 + 0.0000i & -0.0961 + 0.0000i \\ -0.0961 + 0.0000i & 0.0196 + 0.0000i \\ 0.0192 + 0.0000i & 0.0000 - 0.0961i \\ 0.0000 + 0.0961i & 0.4804 + 0.0000i \\ 0.4808 + 0.0000i & -0.0000 + 0.0961i \\ -0.0000 - 0.0961i & 0.0196 + 0.0000i \\ 0.0192 + 0.0000i & -0.0961 - 0.0000i \\ -0.0961 + 0.0000i & 0.4804 + 0.0000i \\ 0.4808 + 0.0000i & 0.0961 + 0.0000i \\ 0.0961 - 0.0000i & 0.0196 + 0.0000i \\ 0.0192 + 0.0000i & -0.0000 + 0.0961i \\ -0.0000 - 0.0961i & 0.4804 + 0.0000i \\ 0.4808 + 0.0000i & 0.0000 - 0.0961i \\ 0.0000 + 0.0961i & 0.0196 + 0.0000i \end{pmatrix},$$

<sup>8</sup>The following statement applies to  $\sigma^S$  and  $\sigma^{US}$ . The first 2x2 matrix represents the (+1|1), the second 2x2 matrix (-1|1), etc.

$$\sigma^{US} = \begin{pmatrix} 0.9608 & 0 \\ 0 & 0 \\ 0.0392 & 0 \\ 0 & 0 \\ 0.9608 & 0 \\ 0 & 0 \\ 0.0392 & 0 \\ 0 & 0 \\ 0.9608 & 0 \\ 0 & 0 \\ 0.0392 & 0 \\ 0 & 0 \\ 0.9608 & 0 \\ 0 & 0 \\ 0.0392 & 0 \\ 0 & 0 \end{pmatrix}.$$

As a calculation step, let us say  $\sigma$  is the 2x2 matrix  $\begin{pmatrix} a & b \\ c & d \end{pmatrix}$ , with  $a, b, c, d \in \mathbb{C}$ . Then:

$$\text{Tr}(\sigma \cdot y_{a|x}) = a \cdot (y_{a|x})^{1,1} + b \cdot (y_{a|x})^{2,1} + c \cdot (y_{a|x})^{1,2} + d \cdot (y_{a|x})^{2,2}.$$

We obtain:

$$\begin{aligned} & -y_0 - 1 + 0.0192 \cdot (y_{1|1})^{1,1} + 0.0961 \cdot (y_{1|1})^{2,1} + 0.0961 \cdot (y_{1|1})^{1,2} + 0.4804 \cdot (y_{1|1})^{2,2} + \\ & 0.4808 \cdot (y_{-1|1})^{1,1} - 0.0961 \cdot (y_{-1|1})^{2,1} - 0.0961 \cdot (y_{-1|1})^{1,2} + 0.0196 \cdot (y_{-1|1})^{2,2} + \\ & 0.0192 \cdot (y_{1|2})^{1,1} - 0.0961i \cdot (y_{1|2})^{2,1} + 0.0961i \cdot (y_{1|2})^{1,2} + 0.4804 \cdot (y_{1|2})^{2,2} + \\ & 0.4808 \cdot (y_{-1|2})^{1,1} + 0.0961i \cdot (y_{-1|2})^{2,1} - 0.0961i \cdot (y_{-1|2})^{1,2} + 0.0196 \cdot (y_{-1|2})^{2,2} + \\ & 0.0192 \cdot (y_{1|3})^{1,1} - 0.0961 \cdot (y_{1|3})^{2,1} - 0.0961 \cdot (y_{1|3})^{1,2} + 0.4804 \cdot (y_{1|3})^{2,2} + \\ & 0.4808 \cdot (y_{-1|3})^{1,1} + 0.0961 \cdot (y_{-1|3})^{2,1} + 0.0961 \cdot (y_{-1|3})^{1,2} + 0.0196 \cdot (y_{-1|3})^{2,2} + \\ & 0.0192 \cdot (y_{1|4})^{1,1} + 0.0961i \cdot (y_{1|4})^{2,1} - 0.0961i \cdot (y_{1|4})^{1,2} + 0.4804 \cdot (y_{1|4})^{2,2} + \\ & 0.4808 \cdot (y_{-1|4})^{1,1} - 0.0961i \cdot (y_{-1|4})^{2,1} + 0.0961i \cdot (y_{-1|4})^{1,2} + 0.0196 \cdot (y_{-1|4})^{2,2} \geq 0. \end{aligned}$$

As well as:

$$-y_0 + 0.9608 \cdot (y_{1|1})^{1,1} + 0.0392 \cdot (y_{-1|1})^{1,1} + 0.9608 \cdot (y_{1|2})^{1,1} + 0.0392 \cdot (y_{-1|2})^{1,1} + 0.9608 \cdot (y_{1|3})^{1,1} + 0.0392 \cdot (y_{-1|3})^{1,1} + 0.9608 \cdot (y_{1|4})^{1,1} + 0.0392 \cdot (y_{-1|4})^{1,1} \geq 0.$$

Implementing this D-SDP in MATLAB gives very similar results for the different matrices as in the previous appendix section. The code snippet can be found in the appendix section C.3.3.

```

1
2
3 F1 =
4
5 -0.4196 - 0.0000i    2.0562 + 0.0000i
6  2.0564 - 0.0001i  -30.2304 - 0.0000i
7
8
9 F2 =
10
11 -0.4196 - 0.0000i   -0.0000 + 0.0000i
12  0.0003 - 0.0001i  -40.3071 - 0.0000i
13
14
15 F3 =
16
17  0.0000 + 0.0000i    0.0000 - 2.0562i
18 -0.0000 + 2.0567i   10.0768 + 0.0000i
19
20
21 F4 =
22
23 1.0e-03 *
24
25  0.0000 + 0.0000i    0.0011 - 0.0003i
26 -0.0003 + 0.5271i    0.0656 + 0.0000i
27
28
29 F5 =
30
31 -0.0000 + 0.0000i   -2.0562 - 0.0000i
32 -2.0565 + 0.0001i   10.0768 + 0.0000i
33
34

```

```

35 F6 =
36
37 1.0e-03 *
38
39 -0.0000 + 0.0000i  0.0013 - 0.0002i
40 -0.2736 + 0.0530i  0.0562 + 0.0000i
41
42
43 F7 =
44
45 -0.0000 - 0.0000i  0.0000 + 2.0562i
46  0.0000 - 2.0567i  10.0768 + 0.0000i
47
48
49 F8 =
50
51 1.0e-03 *
52
53 -0.0000 - 0.0000i  0.0014 - 0.0001i
54  0.0104 - 0.5159i  0.0656 + 0.0000i
55
56
57 Grprime =
58
59 -0.4196 + 0.0000i  -0.0000 - 0.0000i
60 -0.0000 + 0.0000i -40.3069 - 0.0000i
61
62
63 G1prime =
64
65  0.0000 + 0.0000i  2.0562 + 0.0000i
66  2.0562 - 0.0000i  10.0767 + 0.0000i
67
68
69 G2prime =
70
71 -0.0000 + 0.0000i  0.0000 - 2.0562i
72  0.0000 + 2.0562i  10.0767 + 0.0000i
73
74
75 G3prime =
76
77  0.0000 + 0.0000i  -2.0562 + 0.0000i
78 -2.0562 - 0.0000i  10.0767 + 0.0000i

```

```

79
80
81 G4prime =
82
83     0.0000 + 0.0000i    0.0000 + 2.0562i
84     0.0000 - 2.0562i   10.0767 + 0.0000i

```

Thus, we have now implemented 3 different methods yielding very similar results each time. Therefore, one could now assume that our initial approach is a valid procedure, in contradiction to Ref.[17].

### C.3.3 MATLAB code

```

1
2 %% we will implement the D-SPD from the Overleaf document to find the dual
   variables
3
4 dB = 2;
5 assemblageS;
6 assemblageUS;
7 cvx_begin SDP quiet
8 cvx_solver SeDuMi %mosek
9 cvx_precision best
10
11     variable y1     complex           % y(+1|1)^(1,1)
12     variable y2     complex           % y(+1|1)^(1,2)
13     variable y3     complex           % y(+1|1)^(2,1)
14     variable y4     complex           % y(+1|1)^(2,2)
15     variable y5     complex           % y(-1|1)^(1,1)
16     variable y6     complex           % y(-1|1)^(1,2)
17     variable y7     complex           % y(-1|1)^(2,1)
18     variable y8     complex           % y(-1|1)^(2,2)
19
20     variable y9     complex           % y(+1|2)^(1,1)
21     variable y10    complex           % y(+1|2)^(1,2)
22     variable y11    complex           % y(+1|2)^(2,1)
23     variable y12    complex           % y(+1|2)^(2,2)
24     variable y13    complex           % y(-1|2)^(1,1)
25     variable y14    complex           % y(-1|2)^(1,2)
26     variable y15    complex           % y(-1|2)^(2,1)
27     variable y16    complex           % y(-1|2)^(2,2)
28
29     variable y17    complex           % y(+1|3)^(1,1)
30     variable y18    complex           % y(+1|3)^(1,2)

```

```

31     variable y19   complex           % y(+1|3)^(2,1)
32     variable y20   complex           % y(+1|3)^(2,2)
33     variable y21   complex           % y(-1|3)^(1,1)
34     variable y22   complex           % y(-1|3)^(1,2)
35     variable y23   complex           % y(-1|3)^(2,1)
36     variable y24   complex           % y(-1|3)^(2,2)
37
38     variable y25   complex           % y(+1|4)^(1,1)
39     variable y26   complex           % y(+1|4)^(1,2)
40     variable y27   complex           % y(+1|4)^(2,1)
41     variable y28   complex           % y(+1|4)^(2,2)
42     variable y29   complex           % y(-1|4)^(1,1)
43     variable y30   complex           % y(-1|4)^(1,2)
44     variable y31   complex           % y(-1|4)^(2,1)
45     variable y32   complex           % y(-1|4)^(2,2)
46
47     variable y0     % y_0
48     variable ytr    % y_tr
49
50     maximise( y0 + ytr )
51
52     yp11 = [y1,y2;y3,y4];
53     ym11 = [y5,y6;y7,y8];
54     yp12 = [y9,y10;y11,y12];
55     ym12 = [y13,y14;y15,y16];
56     yp13 = [y17,y18;y19,y20];
57     ym13 = [y21,y22;y23,y24];
58     yp14 = [y25,y26;y27,y28];
59     ym14 = [y29,y30;y31,y32];
60
61     yi = ytr*eye(2);
62
63     subject to
64     % constraint eq. (21)
65     -yi - ym11 - ym12 - ym13 - ym14 == hermitian_semidefinite(dB);
66     -yi - ym11 - ym12 - ym13 - yp14 == hermitian_semidefinite(dB);
67     -yi - ym11 - ym12 - yp13 - ym14 == hermitian_semidefinite(dB);
68     -yi - ym11 - ym12 - yp13 - yp14 == hermitian_semidefinite(dB);
69     -yi - ym11 - yp12 - ym13 - ym14 == hermitian_semidefinite(dB);
70     -yi - ym11 - yp12 - ym13 - yp14 == hermitian_semidefinite(dB);
71     -yi - ym11 - yp12 - yp13 - ym14 == hermitian_semidefinite(dB);
72     -yi - ym11 - yp12 - yp13 - yp14 == hermitian_semidefinite(dB);
73     -yi - yp11 - ym12 - ym13 - ym14 == hermitian_semidefinite(dB);
74     -yi - yp11 - ym12 - ym13 - yp14 == hermitian_semidefinite(dB);

```

```

75 -yi - yp11 - ym12 - yp13 - ym14 == hermitian_semidefinite(dB);
76 -yi - yp11 - ym12 - yp13 - yp14 == hermitian_semidefinite(dB);
77 -yi - yp11 - yp12 - ym13 - ym14 == hermitian_semidefinite(dB);
78 -yi - yp11 - yp12 - ym13 - yp14 == hermitian_semidefinite(dB);
79 -yi - yp11 - yp12 - yp13 - ym14 == hermitian_semidefinite(dB);
80 -yi - yp11 - yp12 - yp13 - yp14 == hermitian_semidefinite(dB);
81
82 % constraint eq. (22)
83 -y0 - 1 + assemblageS(1,1)*y1 + assemblageS(1,2)*y3 + assemblageS(2,1)*y2
...
84 + assemblageS(2,2)*y4 + assemblageS(3,1)*y5 + assemblageS(3,2)*y7 ...
85 + assemblageS(4,1)*y6 + assemblageS(4,2)*y8 + assemblageS(5,1)*y9 +
...
86 assemblageS(5,2)*y11 + assemblageS(6,1)*y10 + assemblageS(6,2)*y12
+...
87 assemblageS(7,1)*y13 + assemblageS(7,2)*y15 + assemblageS(8,1)*y14 +
...
88 assemblageS(8,2)*y16 + assemblageS(9,1)*y17 + assemblageS(9,2)*y19
+...
89 assemblageS(10,1)*y18 + assemblageS(10,2)*y20 + assemblageS(11,1)*y21
...
90 + assemblageS(11,2)*y23 + assemblageS(12,1)*y22 + assemblageS(12,2)*
y24 ...
91 + assemblageS(13,1)*y25 + assemblageS(13,2)*y27 + assemblageS(14,1)*
y26...
92 + assemblageS(14,2)*y28 + assemblageS(15,1)*y29 + assemblageS(15,2)*
y31 ...
93 + assemblageS(16,1)*y30 + assemblageS(16,2)*y32 ...
94 == hermitian_semidefinite(1);
95
96 % constraint eq. (23)
97 -y0 + assemblageUS(1,1)*y1 + assemblageUS(3,1)*y5 + assemblageUS(5,1)*y9
...
98 + assemblageUS(7,1)*y13 + assemblageUS(9,1)*y17 + assemblageUS(11,1)*
y21...
99 + assemblageUS(13,1)*y25 + assemblageUS(15,1)*y29 ...
100 == hermitian_semidefinite(1);
101
102 cvx_end
103 cvx_status
104 %cvx_optval
105
106 % The y elements represent the dual variables of the D-SPD:
107 %diary myDiaryfile

```



```
108
109 %diary on
110
111 F1 = yp11 % F(+1,1)
112 F2 = ym11 % F(-1,1)
113 F3 = yp12 % F(+1,2)
114 F4 = ym12 % F(-1,2)
115 F5 = yp13 % F(+1,3)
116 F6 = ym13 % F(-1,3)
117 F7 = yp14 % F(+1,4)
118 F8 = ym14 % F(-1,4)
119
120
121 Grprime = F2 + F4 + F6 + F8
122
123 G1prime = F1 - F2
124 G2prime = F3 - F4
125 G3prime = F5 - F6
126 G4prime = F7 - F8
127
128 %diary off
```

## D Wigner function

In this section, we seek to find a "Bell-like" inequality for the considered state  $\rho$  (3) in terms of Wigner function values.

### D.1 Definition of Wigner function

According to the Heisenberg uncertainty principle, it is impossible to precisely measure a particle's position and momentum at the same time in quantum theory, i.e. to find a phase point in the phase space. Therefore, to examine the quantum state and motion of microscopic particles, scientists searched to define the quasi-distribution function in phase space. In 1932, Eugene Wigner introduced such a quasi-classical distribution function, whose marginal distributions correspond to the particle probability measured in coordinate space  $q$  and momentum space  $p$ . In addition, the Wigner function has an unusual property which makes it a good diagnostic of quantum properties: it may be negative in some sections of phase space when the field includes nonclassical interferences<sup>9</sup>.

The Wigner function  $W(q, p)$  is usually expressed in the following integral form, given the density matrix  $\rho$  of a quantum particle moving in one dimension [32]:

$$W(q, p) = \frac{1}{\pi\hbar} \int \langle q - x | \rho | q + x \rangle \exp(2ipx/\hbar) dx. \quad (97)$$

However, this is not always easy to compute, since given a density matrix, computing quasi-probabilities is a time-consuming job that requires integration over phase-space variables. Therefore, scientists such as for instance Wünsche [33], Moya-Cessa [34] and Cahill [35] sought to derive alternative expressions.

In our case, we will consider the joint 2-mode Wigner function  $W_J(\rho, \beta_A, \beta_B)$ , which is a continuous-variable representation of the considered quantum state with  $\beta_A$  and  $\beta_B$  being complex variables in Alice's and Bob's system respectively. Here,  $W_J$  describes a 4-dimensional phase space function, whose value at each point  $(\text{Re}(\beta_A), \text{Im}(\beta_A), \text{Re}(\beta_B), \text{Im}(\beta_B))$  is equal to the expectation value of the joint parity operator  $P_J$  after independent displacements in Alice's and Bob's system after rescaling by  $\pi^2/4$  [36]. A full quantum state tomography for the two cavity system between them can then be realized by measuring the joint Wigner function. With the aim of doing so, we first require to write the density

---

<sup>9</sup>Although of course not all nonclassical field states have negative contributions to their Wigner functions.

matrix  $\rho$  in the tensor Fock state basis, i.e.:

$$\rho = \sum_{i,j,k,l} \rho_{ijkl} |i, j\rangle \langle k, l|. \quad (98)$$

Subsequently, the linearity of  $W_J$  in  $\rho$  can then be used to compute the individual contribution from each component  $\rho_{ijkl}$  [36]:

$$W_J(\rho, \beta_A, \beta_B) = \frac{4}{\pi^2} \sum_{ijmn} \rho_{i,j,m,n} K_{mi}(\beta_A) K_{nj}(\beta_B). \quad (99)$$

The matrix elements  $K_{mn}(\beta)$  are given by:

$$K_{mn}(\beta) = e^{-|\beta|^2} (-1)^m (2\beta)^{(n-m)} \sqrt{\frac{m!}{n!}} L_m^{(n-m)}(|\beta|), \quad (100)$$

where  $L_m^{(n-m)}$  represent the generalized Laguerre polynomials [37].

## D.2 Analytical computation

In order to compute the joint two-mode Wigner function, we first write our density matrix  $\rho$  (3) in two parts:

$$\rho(\eta) = \eta \underbrace{|\Psi\rangle \langle \Psi|}_{\rho_1} + (1 - \eta) \underbrace{|0, 0\rangle \langle 0, 0|}_{\rho_2}, \quad (101)$$

where

$$|\Psi\rangle = \frac{1}{\sqrt{2}} (|0, 1\rangle + |1, 0\rangle). \quad (102)$$

Thus, we acquire  $\rho$  in the correct form (98), with:

$$\rho_1 = \frac{1}{2} [|0, 1\rangle \langle 0, 1| + |0, 1\rangle \langle 1, 0| + |1, 0\rangle \langle 0, 1| + |1, 0\rangle \langle 1, 0|], \quad (103)$$

$$\rho_2 = |0, 0\rangle \langle 0, 0|. \quad (104)$$

This enables us now to compute the appropriate matrix elements (100) with the initial con-

ditions  $L_0^{(\alpha)} = 1$  and  $L_1^{(\alpha)}(x) = 1 + \alpha - x$  [37]:

$$K_{00}(\beta) = e^{-|\beta|^2}, \quad (105)$$

$$K_{10}(\beta) = \frac{|\beta|}{2\beta} e^{-|\beta|^2}, \quad (106)$$

$$K_{01}(\beta) = 2\beta e^{-|\beta|^2}, \quad (107)$$

$$K_{11}(\beta) = (|\beta| - 1)e^{-|\beta|^2}. \quad (108)$$

This then gives the desired Wigner function:

$$\begin{aligned} W_J(\eta, \beta_A, \beta_B) &= \eta \frac{4}{2\pi^2} [K_{00}(\beta_A)K_{11}(\beta_B) + K_{10}(\beta_A)K_{01}(\beta_B) + K_{01}(\beta_A)K_{10}(\beta_B) \\ &\quad + K_{11}(\beta_A)K_{00}(\beta_B)] + (1 - \eta) \frac{4}{\pi^2} [K_{00}(\beta_A)K_{00}(\beta_B)] \\ &= \eta \frac{2}{\pi^2} [e^{-|\beta_A|^2 - |\beta_B|^2} (|\beta_B| - 1) + \frac{|\beta_A|\beta_B^2 + |\beta_B|\beta_A^2}{\beta_A\beta_B} e^{-|\beta_A|^2 - |\beta_B|^2} \\ &\quad + (|\beta_A| - 1)e^{-|\beta_A|^2 - |\beta_B|^2}] + (1 - \eta) \frac{4}{\pi^2} [e^{-|\beta_A|^2 - |\beta_B|^2}] \end{aligned} \quad (109)$$

### D.3 Bell's Inequality and Wigner Function

The typical CHSH Bell inequalities cannot be applied directly in the setting of non-local two-mode states with continuous variables over a 4-dimensional phase space. Nevertheless, it is possible to write simple inequalities that have the form of a Bell inequality by discretizing the field observables [38, 39]. According to Banaszek and Wódkiewicz [27] and Jeong [28], any local representation of reality should yield measurements that satisfy the following inequality:

$$\mathcal{B} = |\Pi(\alpha', \beta') + \Pi(\alpha, \beta') + \Pi(\alpha', \beta) - \Pi(\alpha, \beta)| \leq \sqrt{2}, \quad (110)$$

with  $\Pi(\alpha, \beta) = \frac{\pi^2}{4} W_J(\alpha, \beta)$  being a scaled version of the joint 2-mode Wigner function (99) at the point in the 4-dimensional phase space defined by the complex amplitudes  $\alpha$  and  $\beta$ . Thus, the *Bell signal*  $\mathcal{B}$  in our case is given by the above equation, inserting (109).

Consequently, local theories impose the bound:

$$-2 \leq \mathcal{B} \leq 2. \quad (111)$$

## References

- [1] Chen, J.-L., Ren, C., Chen, C., Ye, X.-J., & Pati, A. K. (2016). Bell's Nonlocality Can be Detected by the Violation of Einstein-Podolsky-Rosen Steering Inequality. *Scientific Reports*, 6(1). <https://doi.org/10.1038/srep39063>
- [2] Kogias, I. (n.d.). Entanglement, Einstein-Podolsky-Rosen steering and cryptographical applications. Retrieved from [http://eprints.nottingham.ac.uk/34584/1/I.Kogias\\_PhD\\_CorrectedVersion.pdf](http://eprints.nottingham.ac.uk/34584/1/I.Kogias_PhD_CorrectedVersion.pdf)
- [3] Wiseman, H. M., Jones, S. J., & Doherty, A. C. (2007). Steering, Entanglement, Nonlocality, and the Einstein-Podolsky-Rosen Paradox. *Physical Review Letters*, 98(14). <https://doi.org/10.1103/physrevlett.98.14040>
- [4] Cavalcanti, E. G., Jones, S. J., Wiseman, H. M., & Reid, M. D. (2009). Experimental criteria for steering and the Einstein-Podolsky-Rosen paradox. *Physical Review A*, 80(3). <https://doi.org/10.1103/physreva.80.032112>
- [5] Cavalcanti, E. G., & Reid, M. D. (2007). Uncertainty relations for the realization of macroscopic quantum superpositions and EPR paradoxes. *Journal of Modern Optics*, 54(16-17), 2373–2380. <https://doi.org/10.1080/09500340701639623>
- [6] Cavalcanti, D., & Skrzypczyk, P. (2016). Quantum steering: a review with focus on semidefinite programming. *Reports on Progress in Physics*, 80(2), 024001. <https://doi.org/10.1088/1361-6633/80/2/024001>
- [7] Wikipedia Contributors. (2022, March 19). EPR paradox. Wikipedia; Wikimedia Foundation. [https://en.wikipedia.org/wiki/EPR\\_paradox](https://en.wikipedia.org/wiki/EPR_paradox)
- [8] Uola, R., Costa, A. C. S., Nguyen, H. C., & Gühne, O. (2020). Quantum steering. *Reviews of Modern Physics*, 92(1). <https://doi.org/10.1103/revmodphys.92.015001>
- [9] Skrzypczyk, P., Navascués, M., & Cavalcanti, D. (2014). Quantifying Einstein-Podolsky-Rosen Steering. *Physical Review Letters*, 112(18). <https://doi.org/10.1103/physrevlett.112.180404>
- [10] Pusey, M. F. (2013). Negativity and steering: A stronger Peres conjecture. *Physical Review A*, 88(3). <https://doi.org/10.1103/physreva.88.032313>
- [11] Bub, J. (2019). Quantum Entanglement and Information (Stanford Encyclopedia of Philosophy). Retrieved May 15, 2022, from Stanford.edu website: <https://plato.stanford.edu/entries/qt-entangle/>

- [12] Bellt. (1964). ON THE EINSTEIN PODOLSKY ROSEN PARADOX\*. *Physics*, 1(3), 195–290. Retrieved from [https://cds.cern.ch/record/111654/files/vol1p195-200\\_001.pdf](https://cds.cern.ch/record/111654/files/vol1p195-200_001.pdf)
- [13] Einstein, A., Podolsky, B., & Rosen, N. (1935). Can Quantum-Mechanical Description of Physical Reality Be Considered Complete? *Physical Review*, 47(10), 777–780. <https://doi.org/10.1103/physrev.47.777>
- [14] The Einstein-Podolsky-Rosen Argument and the Bell Inequalities. (n.d.). Retrieved from <https://iep.utm.edu/wp-content/media/epr-pdf.pdf>
- [15] Papers with Code - Experimental EPR-Steering of Bell-local States. (2022). Retrieved May 25, 2022, from Paperswithcode.com website: <https://physics.paperswithcode.com/paper/experimental-epr-steering-of-bell-local>
- [16] Quintino, M. T., Vértesi, T., Cavalcanti, D., Augusiak, R., Demianowicz, M., Acín, A., & Brunner, N. (2015). Inequivalence of entanglement, steering, and Bell nonlocality for general measurements. *Physical Review A*, 92(3). <https://doi.org/10.1103/physreva.92.032107>
- [17] Guerreiro, T., Monteiro, F., Martin, A., Brask, J. B., Vértesi, T., Korzh, B., Caloz, M., Bussi eres, F., Verma, V. B., Lita, A. E., Mirin, R. P., Nam, S. W., Marsilli, F., Shaw, M. D., Gisin, N., Brunner, N., Zbinden, H., & Thew, R. T. (2016). Demonstration of Einstein-Podolsky-Rosen Steering Using Single-Photon Path Entanglement and Displacement-Based Detection. *Physical Review Letters*, 117(7).<https://doi.org/10.1103/physrevlett.117.070404>
- [18] Dehlinger, D., & Mitchell, M. W. (2002). Entangled photons, nonlocality, and Bell inequalities in the undergraduate laboratory. *American Journal of Physics*, 70(9), 903–910. <https://doi.org/10.1119/1.1498860>
- [19] Pusey, M. F. (2013). Negativity and steering: A stronger Peres conjecture. *Physical Review A*, 88(3). <https://doi.org/10.1103/physreva.88.032313>
- [20] Quantum steering for more precise measurements. (2021). Retrieved May 15, 2022, from Unibas.ch website: <https://www.unibas.ch/en/News-Events/News/Uni-Research/Quantum-steering-for-more-precise-measurements.html>
- [21] Weston, M. M., Slussarenko, S., Chrzanowski, H. M., Wollmann, S., Shalm, L. K., Verma, V. B., . . . Pryde, G. J. (2018). Heralded quantum steering over a high-loss channel. *Science Advances*, 4(1). <https://doi.org/10.1126/sciadv.1701230>

- [22] Wikipedia Contributors. (2022, March 20). Semidefinite programming. Wikipedia; Wikimedia Foundation. [https://en.wikipedia.org/wiki/Semidefinite\\_programming](https://en.wikipedia.org/wiki/Semidefinite_programming)
- [23] Semidefinite Programming. (2022). Retrieved May 16, 2022, from Stanford.edu website: <https://web.stanford.edu/~boyd/papers/sdp.html>
- [24] Vandenberghe, L., & Boyd, S. (1996). Semidefinite Programming. *SIAM Review*, 38(1), 49–95. <https://doi.org/10.1137/1038003>
- [25] CVX: Matlab Software for Disciplined Convex Programming — CVX Research, Inc. (2012, September 4). Retrieved May 10, 2022, from [Cvxr.com website:http://cvxr.com/cvx/](http://cvxr.com/cvx/)
- [26] Skrzypczyk, P., Navascués, M., & Cavalcanti, D. (2014). Quantifying Einstein-Podolsky-Rosen Steering. *Physical Review Letters*, 112(18). <https://doi.org/10.1103/physrevlett.112.180404>
- [27] Banaszek, K., & Wódkiewicz, K. (1999). Testing Quantum Nonlocality in Phase Space. *Physical Review Letters*, 82(10), 2009–2013. <https://doi.org/10.1103/physrevlett.82.2009>
- [28] Jeong, H., Son, W., Kim, M. S., Ahn, D., & Brukner, Č. (2003). Quantum nonlocality test for continuous-variable states with dichotomic observables. *Physical Review A*, 67(1). <https://doi.org/10.1103/physreva.67.012106>
- [29] Wikipedia Contributors. (2022, March 29). Coherent state. Wikipedia; Wikimedia Foundation. [https://en.wikipedia.org/wiki/Coherent\\_state](https://en.wikipedia.org/wiki/Coherent_state)
- [30] QuIC Seminar 6 Quantum States and Partial Trace. (n.d.). Retrieved from <https://www.ryanlarose.com/uploads/1/1/5/8/115879647/quic06-states-trace.pdf>
- [31] Partial trace. (n.d.). Retrieved from [http://www.thphy.uni-duesseldorf.de/~ls3/teaching/1515-QQI/Additional/partial\\_trace.pdf](http://www.thphy.uni-duesseldorf.de/~ls3/teaching/1515-QQI/Additional/partial_trace.pdf)
- [32] Wootters, W. K. (2004). Picturing qubits in phase space. *IBM Journal of Research and Development*, 48(1), 99–110. <https://doi.org/10.1147/rd.481.0099>
- [33] Wunsche, A. (1991). Displaced Fock states and their connection to quasiprobabilities. *Quantum Optics: Journal of the European Optical Society Part B*, 3(6), 359–383. <https://doi.org/10.1088/0954-8998/3/6/005>

- [34] Moya-Cessa, H., & Knight, P. L. (1993). Series representation of quantum-field quasiprobabilities. *Physical Review A*, 48(3), 2479–2481. <https://doi.org/10.1103/physreva.48.2479>
- [35] Cahill, K. E., & Glauber, R. J. (1969). Density Operators and Quasiprobability Distributions. *Physical Review*, 177(5), 1882–1902. <https://doi.org/10.1103/physrev.177.1882>
- [36] Wang, C., Gao, Y. Y., Reinhold, P., Heeres, R. W., Ofek, N., Chou, K., ... Schoelkopf, R. J. (2016). A Schrödinger cat living in two boxes. *Science*, 352(6289), 1087–1091. <https://doi.org/10.1126/science.aaf2941>
- [37] Kim, T., Dolgy, D. V., Kim, D. S., Kim, H. K., & Park, S. H. (2021). A note on degenerate generalized Laguerre polynomials and Lah numbers. *Advances in Difference Equations*, 2021(1). <https://doi.org/10.1186/s13662-021-03574-8>
- [38] Milman, P., Auffeves, A., Yamaguchi, F., Brune, M., Raimond, J. M., & Haroche, S. (2004). A proposal to test Bell's inequalities with mesoscopic non-local states in cavity QED. *The European Physical Journal D*, 32(2), 233–239. <https://doi.org/10.1140/epjd/e2004-00171-6>
- [39] Banaszek, K., & Wódkiewicz, K. (1999). Testing Quantum Nonlocality in Phase Space. *Physical Review Letters*, 82(10), 2009–2013. <https://doi.org/10.1103/physrevlett.82.2009>